

Master Thesis

# Characterization of *Trichodesmium* Filament-Filament Interactions and their Effect on Aggregate Behavior

Giulia Schneider

## Supervision

Prof. Dr. Roman Stocker  
Dr. Ulrike Pfreundt

April 15, 2019



Eidgenössische Technische Hochschule Zürich  
Swiss Federal Institute of Technology Zurich

## Declaration of originality

The signed declaration of originality is a component of every semester paper, Bachelor's thesis, Master's thesis and any other degree paper undertaken during the course of studies, including the respective electronic versions.

Lecturers may also require a declaration of originality for other written papers compiled for their courses.

---

I hereby confirm that I am the sole author of the written work here enclosed and that I have compiled it in my own words. Parts excepted are corrections of form and content by the supervisor .

**Title of work** (in block letters):

Characterization of *Trichodesmium* Filament-Filament Interactions and their Effect on Aggregate Behavior

**Authored by** (in block letters):

*For papers written by groups the names of all authors are required.*

**Name(s):**

Schneider

**First name(s):**

Giulia

With my signature I confirm that

- I have committed none of the forms of plagiarism described in the '[Citation etiquette](#)' information sheet.
- I have documented all methods, data and processes truthfully.
- I have not manipulated any data.
- I have mentioned all persons who were significant facilitators of the work .

I am aware that the work may be screened electronically for plagiarism.

**Place, date**

Zürich, April 15, 2019

**Signature(s)**

*G. Schneider*

*For papers written by groups the names of all authors are required. Their signatures collectively guarantee the entire content of the written paper.*

# Abstract

The filamentous, nitrogen-fixing cyanobacteria *Trichodesmium* spp. exist in the oligotrophic tropical oceans where the genus sustains primary phytoplankton production through the active release of nutrients. *Trichodesmium* spp. form dynamic aggregates of hundreds of filaments. Filaments can adjust aggregate shape and density by gliding on other filaments. The processes of experimental aggregate formation and aggregate behavior are currently not understood. Filament pairs have been observed to frequently reverse when they are about to separate. It is hypothesized that observed filament pair reversals can explain experimental aggregate formation. The objective of this thesis was to quantify filament-filament interactions using image analysis and to explain aggregate formation based on obtained filament pair kinetics.

For this purpose, *Trichodesmium* filaments were imaged in microfluidics chambers at 2x magnification. *Trichodesmium erythraeum* IMS101 cultures in the late exponential growth phase were split into two samples: the aggregating and non-aggregating culture. Aggregate formation in the aggregating culture was induced by adding Menadione, which is a reactive oxygen species generating chemical. For aggregation control, the cultures were in parallel imaged in a macroscopic setup.

An algorithm to segment filament pairs into single filaments was successfully developed and implemented. It separates the filaments based on a combination of distance and intensity thresholding.

*Trichodesmium* filament pairs reverse more often than single filaments; a single filament reverses on average every 40 minutes, whereas filament pairs reverse every 12 minutes. Reversals in filament pairs are dependent on lack of overlap (*LOL*). Thus, filaments in filament pairs reverse either actively by sensing *LOL* or passively through some restoring force associated with *LOL*. The fraction of reversing pairs decreases with increasing relative filament velocity. Filaments might need a certain signaling time to reverse or faster filaments might be in a different, actively separating, physiological state.

No difference in reversal frequency and *LOL* at reversal points was observed between the aggregating and non-aggregating cultures. Filament pairs in aggregating cultures had on average a 24 % lower relative velocity than pairs in non-aggregating cultures samples. The mean interaction time of filament pairs was about 1.5 times longer in aggregating than in non-aggregating cultures. The differences between cultures do not explain observed experimental aggregate formation conclusively. As a next step, modeling of *Trichodesmium* filament with the obtain filament kinetics is necessary to understand aggregate formation.

We discovered a novel mechanism of *LOL*-triggered reversals triggered by quantifying filament-filament interactions. Experimental aggregate formation was not conclusively explained in this project, but modeling of filament is necessary. This thesis is part of a broader research project of *Trichodesmium* self-assembly by Dr. Ulrike Pfreundt.

## Acknowledgments

This diverse project has been a challenging and enriching experience. It would not have been possible and would not have been as exciting without the following persons.

My special thanks to Dr. Ulrike Pfreundt, my official supervisor, for her valuable insights into *Trichodesmium* biology and her encouraging supervision. Many thanks also to Dr. Jonasz Slomka, my second unofficial supervisor, for his explanations of encounter rates and filament modeling approaches and his many valuable suggestions. I thank you both for your enthusiasm for the project and many productive discussions - it has been a great pleasure working with you.

I would like to thank Prof. Dr. Roman Stocker for his useful and constructive propositions on this project. I would also like to express my gratitude to Ela Burmeister for her help and patience in the lab.

I thank Claudia Leuch, Dr. Patrick Mathys, Dr. Ulrike Pfreundt, Thomas Kleiven and Daniel Schneider for their highly appreciated feedback on the manuscript.

Last but not least, I thank my parents, Maria Chiara Saraceni and Daniel Schneider, for their ongoing moral support.

# Table of contents

<b>1</b>	<b>Introduction</b>	<b>1</b>
<b>2</b>	<b>Material and methods</b>	<b>3</b>
2.1	<i>Trichodesmium erythraeum</i> IMS101 cultures . . . . .	3
2.2	Experimental setup . . . . .	3
2.2.1	Treatment of <i>Trichodesmium</i> cultures . . . . .	4
2.2.2	Imaging of filament pair interactions . . . . .	4
2.2.3	Aggregation control . . . . .	5
2.3	Particle tracking . . . . .	6
2.3.1	Segmentation . . . . .	6
2.3.2	Linking, merging and splitting . . . . .	7
2.3.3	Track classification . . . . .	7
2.3.4	Performance . . . . .	8
2.4	Segmentation of filament pairs . . . . .	9
2.4.1	Distance transform . . . . .	10
2.4.2	Normed intensity . . . . .	10
2.4.3	Previous overlap weighting . . . . .	10
2.4.4	Distance and intensity threshold parameters . . . . .	10
2.4.5	Overlap region . . . . .	11
2.4.6	Allocation of non-overlap region to filaments . . . . .	11
2.4.7	Performance . . . . .	11
2.5	Calculation of derived quantities . . . . .	12
2.5.1	Measures of overlap . . . . .	12
2.5.2	Velocity . . . . .	12
2.5.3	Reversal frequency . . . . .	12
2.6	Statistics . . . . .	13
2.6.1	Parameter estimation . . . . .	13
2.6.2	Statistical test . . . . .	13
<b>3</b>	<b>Results</b>	<b>14</b>
3.1	Types of filament pair interactions . . . . .	14
3.1.1	Types of relative movement . . . . .	14
3.1.2	Endings of filament pair tracks . . . . .	15
3.1.3	Reversing and non-reversing pairs . . . . .	16
3.2	Kinetics of filament pair interactions . . . . .	19
3.2.1	Relative filament velocity . . . . .	19
3.2.2	Reversal statistics . . . . .	20
3.3	Interaction time . . . . .	22
3.4	Effect of filament pair kinetics on interaction time . . . . .	23

<b>4 Discussion</b>	<b>26</b>
4.1 Reversals . . . . .	26
4.2 Relative filament pair velocity . . . . .	26
4.3 Estimation of filament detachment rate . . . . .	27
4.4 Can differences in filament pair interactions explain macroscopic aggregation? . . . . .	28
4.5 Strengths and limitations of this study . . . . .	28
4.6 Aggregate formation in the ocean . . . . .	29
<b>5 Conclusion</b>	<b>30</b>
<b>References</b>	<b>I</b>
<b>Appendix</b>	<b>II</b>
<b>A Overview of experiments</b>	<b>III</b>
<b>B Distributions of characteristic lengths at reversals points</b>	<b>VII</b>
<b>C Mean squared displacement of single filaments</b>	<b>IX</b>
<b>D Distributions of relative filament velocity and interaction time of different sub-groups</b>	<b>X</b>
<b>E Interaction time statistics</b>	<b>XII</b>
<b>F Estimation of <i>Trichodesmium</i> encounter rates</b>	<b>XIV</b>
F.1 Aggregation control . . . . .	XIV
F.2 In the ocean . . . . .	XIV

# List of figures

1.1	<i>Trichodesmium</i> spp. bloom off the coast of east Australia near Gladstone. . . . .	1
1.2	<i>Trichodesmium erythraeum</i> filaments (a) and aggregates of <i>tuft</i> and <i>puff</i> shape (b). . . . .	2
2.1	Growth curve of <i>Trichodesmium erythraeum</i> IMS101 under described laboratory conditions and light intensities between 40 to 50 $\mu\text{mol}_{\text{photons}} \text{m}^{-2} \text{s}^{-1}$ . . . . .	3
2.2	Design (a) and image (b) of microfluidics chambers. . . . .	4
2.3	Macroscopic aggregation control set-up: non-aggregating and aggregating cultures. . . . .	5
2.4	Particle tracking pipeline . . . . .	6
2.5	Merging and splitting of track segments. (a) Merging and splitting events. (b) Calculation of estimated aggregate centroid. . . . .	8
2.6	Segmentation of overlap region based on distance and intensity thresholding. . . . .	9
2.7	Characteristic measures of overlap. . . . .	12
2.8	Definition of reversals for single filaments (a) and filament pairs (b). . . . .	13
3.1	Types of relative movements in filament pair interactions . . . . .	14
3.2	Filament pair track endings in aggregating and non-aggregating cultures. . . . .	15
3.3	CDF of (a) absolute value of relative filament velocity and (b) interaction time of non-separating and separating tracks. . . . .	15
3.4	Fraction of separating pairs as function of track averaged relative filament velocity in (a) aggregating and (b) non-aggregating cultures. . . . .	16
3.5	Fraction of reversing/non-reversing and separating/non-separating filament pair interactions in aggregating and non-aggregating cultures. . . . .	17
3.6	CDF of (a) absolute value of relative filament velocity and (b) interaction time of reversing and non-reversing tracks. . . . .	17
3.7	Fraction of reversing pairs as function of track averaged relative filament velocity in (a) aggregating and (b) non-aggregating cultures. . . . .	18
3.8	Fraction of reversing pairs as function of summed filament lengths in (a) aggregating and (b) non-aggregating cultures. . . . .	18
3.9	CDF of track averaged (a) absolute single filament velocity and (b) absolute value of relative filament velocity of filament pairs. . . . .	19
3.10	Smoothed, instantaneous overlap velocity (mean $\pm$ std) as function of <i>LOL</i> in (a) aggregating and (b) non-aggregating cultures . . . . .	19
3.11	CDF of normed total gliding distance in (a) reversing and (b) non-reversing pairs comparing aggregating and non-aggregating cultures. . . . .	21
3.12	CDF of <i>LOL</i> at reversal points of (a) non-separating and (b) separating filament pairs comparing aggregating and non-aggregating cultures. . . . .	21
3.13	CDF of filament interaction time <i>t</i> of (a) single filaments and (b) filament pairs comparing aggregating and non-aggregating cultures. . . . .	22
3.14	Effect of total relative gliding distance $d_{\text{glide}}$ on filament pair interaction time. . . . .	24
3.15	Effect of stalling time fraction $f_{\text{stalling}}$ on filament pair interaction time. . . . .	24

3.16 Effect of relative filament velocity $v_r$ on filament pair interaction time. . . . .	25
A.1 Aggregation control experiments: control (top) and Menadione treated (below) samples. . . . .	V
A.1 Aggregation control experiments: control (top) and Menadione treated (below) samples (cont.). . . . .	VI
B.1 CDF of absolute non-overlap length of shorter filament $x_{LOL}$ at reversal points of (a) non-separating and (b) separating filament pairs comparing aggregating and non-aggregating cultures. . . . .	VII
B.2 CDF of non-overlap length of shorter filament normalized by (a) total filament pair and (b) summed filament lengths comparing aggregating and non-aggregating cultures.	VIII
B.3 CDF of (a) absolute and (b) normalized overlap length comparing aggregating and non-aggregating cultures. . . . .	VIII
C.1 Mean square displacement of single filaments. . . . .	IX
D.1 CDF of (a)(c) absolute change in overlap and (b)(d) interaction times of reversing tracks comparing aggregating and non-aggregating cultures. . . . .	X
D.2 CDF of (a)(c) absolute change in overlap and (b)(d) interaction times of non-reversing tracks comparing aggregating and non-aggregating cultures. . . . .	XI
E.1 QQ-Plot comparing filament pair interaction times to a exponential distribution for (a) aggregating and (b) non-aggregating cultures. . . . .	XII
E.2 QQ-Plot comparing filament pair merging times to a exponential distribution for (a) aggregating and (b) non-aggregating cultures. . . . .	XII
E.3 QQ-Plot comparing filament pair separation times to a exponential distribution for (a) aggregating and (b) non-aggregating cultures. . . . .	XIII
E.4 PDF of (a) observed and (b) simulated interaction times of non-separating and separating tracks. . . . .	XIII

# List of tables

3.1	Fraction of relative movement types in aggregating and non-aggregating cultures. . . . .	14
3.2	Mean reversal frequency $f_{rev}$ and mean reversal distance $d_{rev}$ of single filaments and filament pairs in aggregating and non-aggregating cultures. . . . .	20
3.3	Mean track duration $t$ , mean velocity $v$ and the relative difference between cultures (as fraction of the lower value) for different subgroups in aggregating and non-aggregating cultures. . . . .	23
A.1	Overview of conducted experiments. . . . .	IV

# List of abbreviations and symbols

$A_i$	Area of particle $i$
$\mathbf{C}_i$	Centroid of particle $i$
$\mathbf{C}_{jk}$	Computed aggregate centroid of particles $j$ and $k$
CDF	Cumulative distribution function
$c_v$	Coefficient of variation
$d$	Distance transform
$d_{glide}$	Total distance a filament pair glides along each other
$d_{jk}$	Euclidean distance between particles $j$ and $k$
$\bar{e}_i$	Track averaged eccentricity of particle $i$
$f_{rev}$	Overall reversal frequency
$f_{stalling}$	Stalling fraction of filament pair track, i.e. all time steps when $ v_r  < 0.1 \mu\text{m s}^{-1}$
$I$	Normed intensity
$I_{bg}$	Background intensity
$I_{fg}$	Foreground intensity, $I_{fg} = I_{gray} - I_{bg}$
$I_{gray}$	Original image intensity
$LOL$	Lack of overlap
$LOL_{rev}$	$LOL$ at reversal points
$l_1$	Length of filament 1
$l_{1,in}$	Input length of filament 1
$l_1$	Length of filament 2
$l_{2,in}$	Input length of filament 2
$l_{ov}$	Overlap length
$l_t$	Total filament pair length, $l_t = l_1 + l_2 - l_{ov}$
MSD	Mean square displacement
MWU	Mann- Whitney- $U$ -test
$n_{rev}$	Number of reversals
PAR	Photosynthetically active radiation

PDF	Probability distribution function
$Pos$	Position (projection) of the shorter filament's centroid on the longer filament
$R_{max}$	Maximal linking radius
$r_{prev,ov}$	Inverse distance transform of previous overlap region
$t$	Duration
$t_{end}$	End time of particle track
$t_m$	Average encounter time of filament pair with another filament or filament bundle
$t_{merge}$	Merge time of continuous track with single filament
$t_p$	Average filament pair interaction time
$t_s$	Average separation time of particle track
$t_{start}$	Start time of particle track
$t_{split}$	Split time of continuous track into single filament and aggregate track
$Q_{i,p}$	$p$ -Quantile of property $i$
$v_r$	Relative filament pair velocity
$w_{prev,ov,d}$	Weighting function of distance transform $d$
$w_{prev,ov,I}$	Weighting function of normed intensity $I$
$x_{LOL}$	Non-overlapping length of the shorter filament
$\lambda_m$	Encounter rate of filament pair with another filament or filament bundle
$\lambda_p$	Ending rate of filament pair interactions
$\lambda_s$	Separation rate of filament pair interactions

# 1 Introduction

The marine, filamentous, nitrogen-fixing cyanobacteria *Trichodesmium* spp. sustain phytoplankton production through the active release of nitrogen ( $N_2$ ) and organic carbon and are thus of major relevance for marine life, the pelagic food web and global oxygen ( $O_2$ ) production [1][2].  $N_2$  input by *Trichodesmium* spp. (about  $6 \times 10^{10}$  to  $8 \times 10^{10} \text{ kg a}^{-1}$ ) accounts for approximately 25 to 50 % of total marine nitrogen fixation [2][3][4][5]. *Trichodesmium* spp. are found in the warmer and oligotrophic surface waters of the tropical and subtropical oceans [3]. Under favorable conditions, i.e. increased nutrient input, low wind speeds and high temperature, *Trichodesmium* spp. can accumulate in extensive, streaky, sometimes toxic surface blooms, visible on satellite images (figure 1.1) [6][7][8].



**Figure 1.1:** *Trichodesmium* spp. bloom off the coast of east Australia near Gladstone. The image was acquired with the Operational Land Imager on Landsat 8 on September 11, 2017. Image courtesy of Joshua Stevens, NASA Earth Observatory, U.S. Geological Survey [9].

*Trichodesmium* spp. form aggregates of tens to hundreds of trichomes, i.e. single filaments (cf figure 1.2a) [1][6]. Reported fractions of filaments in aggregates to individual filaments in the ocean vary between 10 to 90 % [1][6][10][11]. The percentage of trichomes in aggregates increases during blooms [6]. Two types of aggregate forms are distinguished: fusiform *tufts* and spherical *puffs* (figure 1.2b). Tufts are more commonly observed in the ocean [6][10]. Under laboratory conditions, aggregates form in the stationary growth phases [12][13][14]. Aggregate formation in *Trichodesmium* cultures has generally been associated with stress [12], as for example nutrient depletion [15] or irradiance [12].

The formation of aggregates has various advantages: aggregates promote uptake of iron [16], interactions with bacterial associates [17], and presumably vertical migration for phosphorus mining at depth [18]. A debated possible advantage is the creation of  $O_2$  depleted microenvironments that

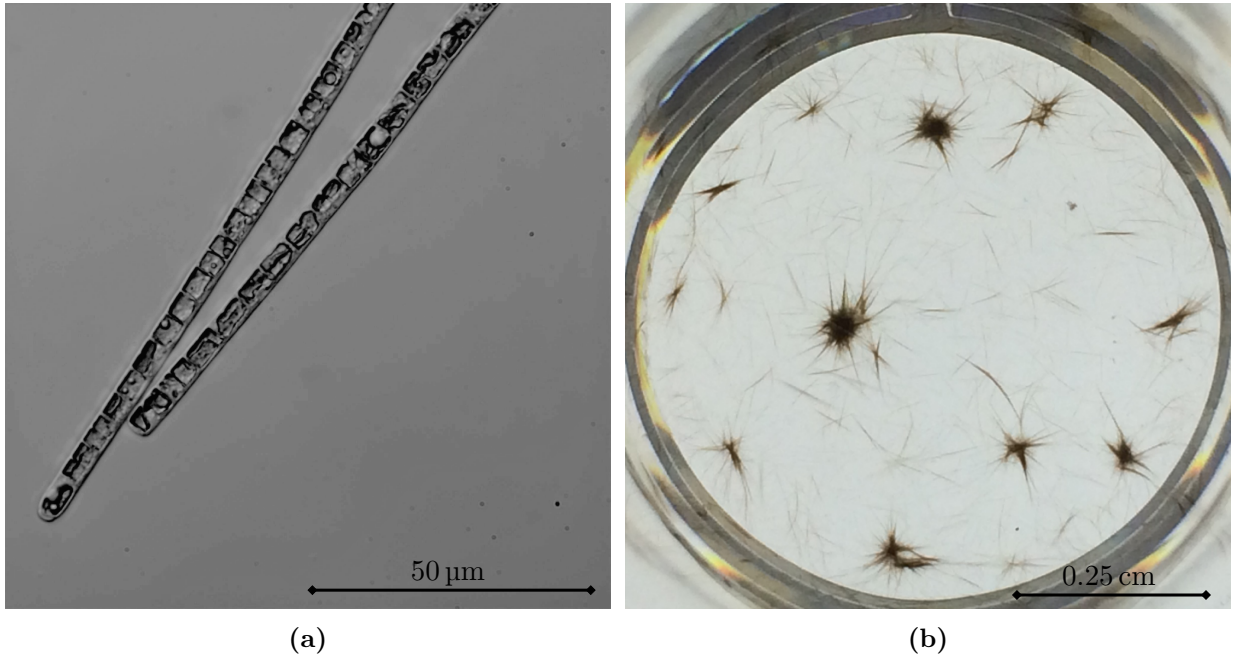


**Figure 1.2:** *Trichodesmium erythraeum* filaments (a) and aggregates of *tuft* and *puff* shape (b). Image courtesy of Ulrike Pfreundt.

would favor the O<sub>2</sub>-sensitive process of N<sub>2</sub>-fixation. However, recent work points to the opposite, aggregates do not increase N<sub>2</sub> fixation [19], since elevated O<sub>2</sub> concentrations during photosynthesis in the aggregate center are disadvantageous for both carbon acquisition and N<sub>2</sub> fixation [20].

Aggregates are dynamic assemblies of *Trichodesmium* filaments and filament motility is an essential component of aggregate behavior. Trichomes can glide on surfaces, which allows them to adjust aggregate shape and density using other filaments as gliding substrate. Similarly, aggregate formation in experimental setups requires motile filaments [15][21]. The cellular gliding mechanism is currently not known [15]. In general, aggregate formation of dispersed particles is statistically expected if encounter times are on average shorter than detachment rates. The specific processes of *Trichodesmium* aggregate formation and behavior remain unexplained.

Filaments in filament pairs have been observed to reverse before they glide apart - they interact through frequent reversals. Based on this observation, it was hypothesized that filament pair reversals can explain experimental aggregate formation and macroscopic aggregate behavior.

The objective of this thesis was to first quantify filament-filament interactions and to then explain experimental aggregate formation based on obtained filament pair kinetics. Filament-filament interactions were quantified using image analysis by developing an algorithm to segment filament pairs into single filaments. Interactions were characterized based on reversals, interaction time and relative filament velocity. To extrapolate from filament pairs to aggregates, we compared pair interactions of *Trichodesmium* cultures in an aggregating and non-aggregating physiological states.

## 2 Material and methods

### 2.1 *Trichodesmium erythraeum* IMS101 cultures

*Trichodesmium erythraeum* IMS101 cultures were used in all experiments. The cultures were grown in modified YBCII medium [22] in Nunc EasYFlask 25 cm<sup>2</sup> cell culture flasks under a 12 h light-dark cycle. They were kept at 25°C in an Algaetron AG230 incubator and were continuously shaken at 160 rpm (Heidolph Unimax 1010 shaker). According to the position on the shaker, the incoming photosynthetically active radiation (PAR) varied between 65 to 85 μmol<sub>photons</sub> m<sup>-2</sup> s<sup>-1</sup>.

We quantified *Trichodesmium* growth at light intensities between 40 to 50 μmol<sub>photons</sub> m<sup>-2</sup> s<sup>-1</sup> as the increase of cumulative filament length per volume ( $l_{cum}/V$ ) over time. After an average lag time of 2 to 3 days, the cultures grew with a doubling time of 4 days (figure 2.1). For irradiances between 65 to 85 μmol<sub>photons</sub> m<sup>-2</sup> s<sup>-1</sup>, the estimated doubling time was about 3 days. *Trichodesmium* cultures were diluted every 14 days, before reaching the stationary growth phase, with a dilution factor of 1:25.

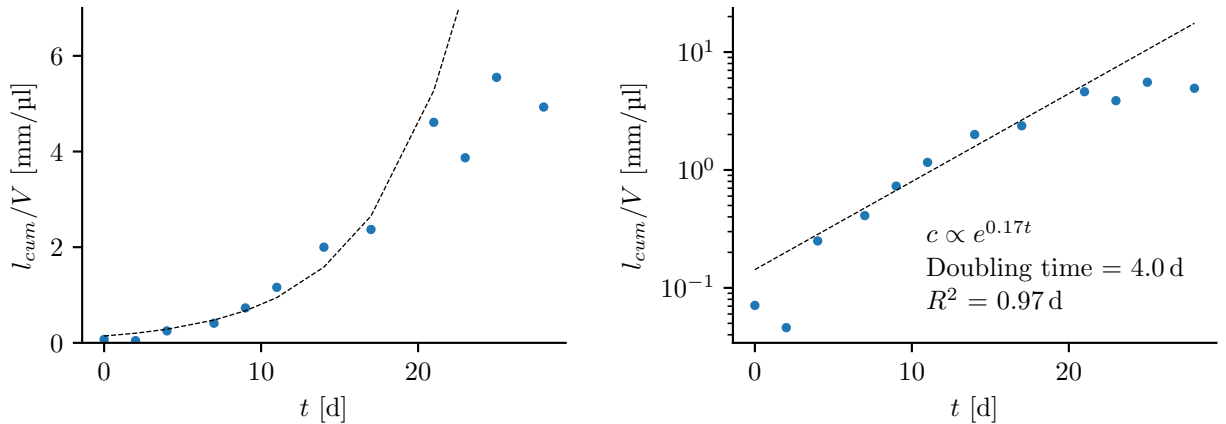


**Figure 2.1:** Growth curve of *Trichodesmium erythraeum* IMS101 under described laboratory conditions and light intensities between 40 to 50 μmol<sub>photons</sub> m<sup>-2</sup> s<sup>-1</sup>. The growth rate was calculated from the cumulative filament length per volume ( $l_{cum}/V$ ) as measure for growth. Given an initial lag time, it was assumed that the exponential growth phase lasted between  $t = 5$  to 21 d.

### 2.2 Experimental setup

Data from several experiments were combined for this analysis, since interactions of exactly two filaments were scarce and not enough data for statistical analysis was collected during a single experiment. Table A.1 in the appendix provides an overview of conducted experiments. The

experimental procedure was standardized to allow comparison among experiments and is described in this section.

### 2.2.1 Treatment of *Trichodesmium* cultures

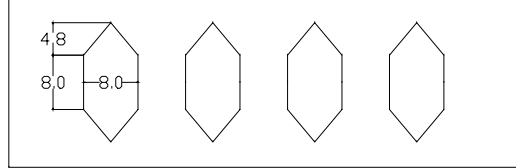
For all experiments, we used *Trichodesmium* cultures in the late exponential growth phase (14 d after dilution) that did not naturally form aggregates, yet. The culture was split into two 5 mL samples:

- Aggregating culture: addition of Menadione (2-Methylnaphthalene-1,4-dione)
- Non-aggregating culture: control sample

Menadione generates reactive oxygen species and induces, in combination with light, aggregate formation in *Trichodesmium* cultures. Based on experience from previous experiments, Menadione was added to the aggregating culture in a concentration of 5  $\mu\text{M}_{\text{Menadione}}$ . After an incubation time of 2 to 4 hours, the cultures were filled into microfluidics chambers for imaging of filament pair interactions. In parallel, the cultures were put into larger wells for macroscopic aggregation control.

### 2.2.2 Imaging of filament pair interactions

Filament pair interactions were imaged in the microfluidics chambers (figure 2.2) at 0.05 fps with 2 $\times$  magnification (Nikon Plan Apo  $\lambda$  objective) on a Nikon Eclipse Ti microscope equipped with an Andor Zyla sCMOS camera. The imaging light intensity, provided by the CoolLED pE-100, was set to 0.6% with an exposure time of 2.2 ms.



(a)



(b)

**Figure 2.2:** Design (a) and image (b) of microfluidics chambers. Units in (a) are given in mm.

An additional LED light source was mounted on the left side to provide enough energy for gliding through photosynthesis. PAR was measured with WALZ light meter ULM 500 using a spherical sensor and varied between 50 to 78  $\mu\text{mol}_{\text{photons}} \text{m}^{-2} \text{s}^{-1}$  depending on measurement position (above or below microfluidics chamber). A temperature of at least 25°C was ensured by the CAGE incubator by Life imaging services.

The chambers were first filled with depletion medium (mYBCII medium without Fe and P) to reduce the number of bubbles entrapped during the filling process. The *Trichodesmium* filaments were then filled with a 1 mL pipette into the chambers, alternating between aggregating and non-aggregating cultures. The filament density inside the chambers was quite difficult to control. In some instances, the filaments sank slowly and were flushed through the chamber. In other cases, the

filaments sank and attached to the microscope slide immediately, which resulted in very high filament densities at the entrance. *Trichodesmium* densities varied between 0.1 to 1.4 filaments mm<sup>-2</sup> with an average of 0.6 filaments mm<sup>-2</sup>. The filament density affects the encounter time between filaments, which is further discussed in section 4.3.

The microfluidics device was made of Polydimethylsiloxane (PDMS) [23]. The PDMS was produced with SYLGARD 184 Base and Curing Agent and bonded to a microscope slide after plasma-treatment. The device was designed for 2× magnification, an image covers about 60 % of the 8×8 mm chamber. Furthermore, the chamber height of 85 µm allows for separation of filaments attached to the microscope slide or to the PDMS by adjusting focus. The master was produced using photolithography with Photoresist SU-8 3000 [24].

### 2.2.3 Aggregation control

For macroscopic aggregation control, 1.5 ml of each culture was placed in a 2 cm<sup>2</sup> well (Falcon Polystyrene Microplates 24 well plate) as shown in figure 2.3. The temperature was kept at 25°C and PAR was set to 73 µmol<sub>photons</sub> m<sup>-2</sup> s<sup>-1</sup>.

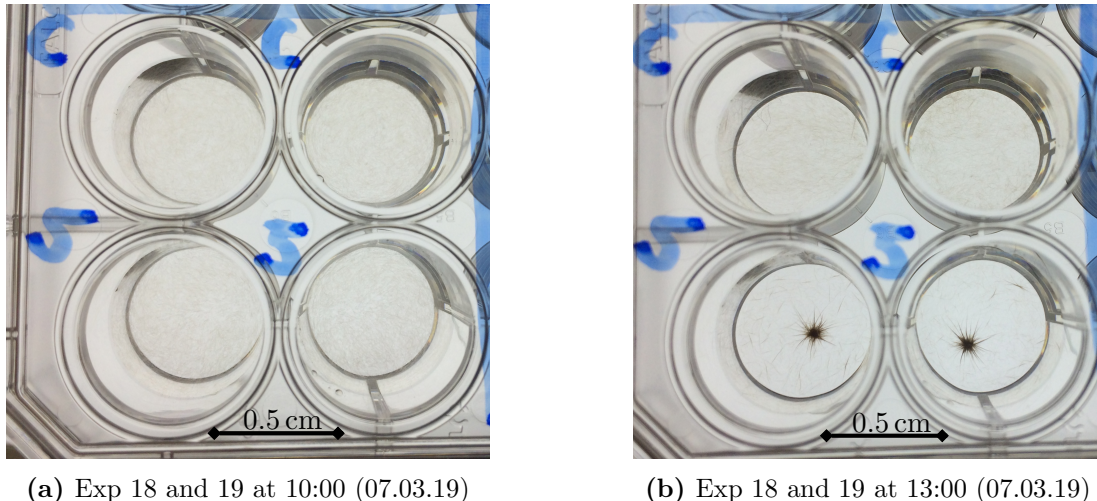


**Figure 2.3:** Macroscopic aggregation control set-up: non-aggregating (top) and aggregating cultures (bottom).

Most filaments were negatively buoyant and sank quickly. *Trichodesmium* density at the well bottom was about 27 filaments mm<sup>-2</sup>, given an average culture concentration of 4 filaments µL<sup>-1</sup> and assuming that 90 % of filaments sank to the bottom. Given equation F.1 in appendix F.1, the average time between two filament encounters is 195 s in the aggregating culture sample and 160 s in the non-aggregating sample.

The Menadione-treated culture samples aggregated in all experiments, aggregates were first visible after 20 minutes to 2 hours (cf. table A.1). The aggregates of experiment 12 (15.02.2019) were not fully contractile; the generated data was not discarded, since an aggregating trend was observed. The control culture samples did not aggregate in any experiment. All aggregation control images are shown in figure A.1.

## 2.3 Particle tracking

In a first processing step, all particles were tracked, classified and extracted from the generated image sequences following the steps in figure 2.4. In a second step, tracks of filament pairs were further segmented as described in section 2.4. The pixel size of captured images was  $3.24 \mu\text{m px}^{-1}$ .

The processing software was written in Python 3 (version 3.6.7) and requires the following packages:

- OpenCV 4.0.0 [25]
- Numpy 1.16.0
- Scipy 1.2.0
- Pandas 0.23.4

All processing was run on a DELL Inspiron 5559 Laptop with 4 Intel Core i7 2.5 GHz processors.

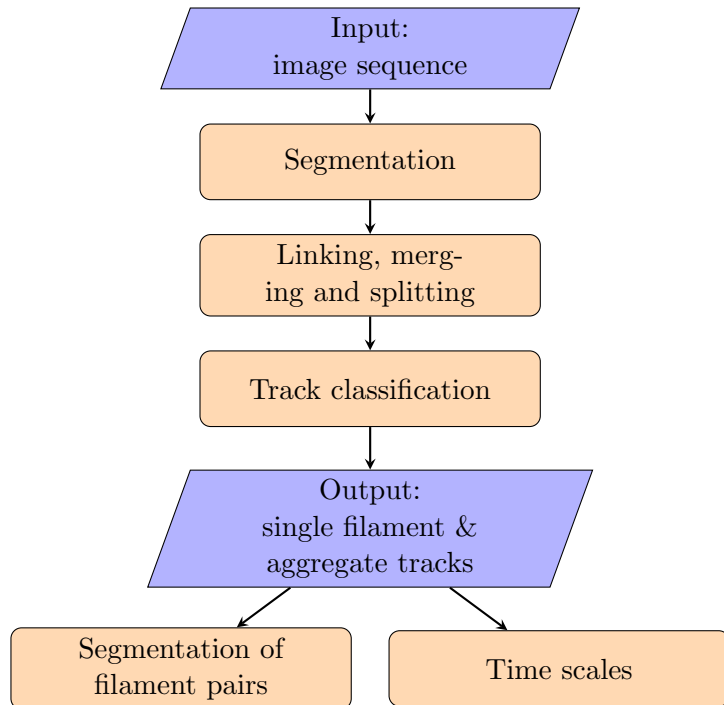


**Figure 2.4:** Particle tracking pipeline

### 2.3.1 Segmentation

The images were segmented into moving objects (foreground) and background by subtracting the median background image followed by thresholding. The median background image was only calculated with 10 % of all images to reduce computational time. The images were previously smoothed with a  $7 \times 7$  Gaussian filter to reduce light variations. If filament densities inside the chamber were very high, the median background image contained filament residuals and was manually corrected with GIMP (GNU Image Manipulation Program, version 2.8.22).

The segmentation threshold was chosen based on trial-and-error and varied between 25 to 45 gray value intensity (8-bit) of the foreground image depending on lighting conditions. We discarded

particles close to the image border or microfluidics chamber wall (within a distance of 20 pixel) due to high noise probability.

### 2.3.2 Linking, merging and splitting

The detected particles in different frames were connected to particle tracks by first linking particles between subsequent frames and then linking track segments over multiple frames. Due to the low particle density, a simple nearest neighbor matching scheme was implemented to link particles or track segments [26]. The scheme links particles  $j$  in frame  $t$  with particles  $k$  in frame  $t + i$  in the order of ascending cost up to a maximal linking distance  $R_{max}$ . Since filaments move little between frames, the cost function was set to the Euclidean distance  $d_{jk}$  between the particles' centroids in frames  $t$  and  $t + i$ .

Particles were linked between subsequent frames up to a maximal distance of 5 pixels, which corresponds to about 16  $\mu\text{m}$ . Track segment ends were connected to track segments starting between 1 to 4 frames later, if the cost did not exceed  $R_{max} = 40$  pixels (130  $\mu\text{m}$ ) and the length difference between particles  $j$  and  $k$  was smaller than 20 pixels (65  $\mu\text{m}$ ).

Since this analysis was mainly focused on filament pair interactions, a merging and splitting algorithm was implemented to flag particle tracks consisting of two or more filaments. The flagged aggregate tracks and respective merged or split track numbers were stored for track classification (section 2.3.3). Four possible types of particle merging and splitting were distinguished: (1) two ending tracks merge into one starting track, (2) one ending track merges with a continuous track, (3) one ending track splits into two starting tracks, (4) one starting track splits from the middle on another track (figure 2.5a) [27]. For events (2) and (4), the continuous track was split into a single filament and aggregate track.

The merging and splitting algorithm iterates through all frames in which a track segment ends ( $t_{end}$ ) or starts ( $t_{start}$ ) and evaluates first splitting and then merging events. If the minimal distance between the bounding boxes of particles  $j$  and  $k$  in frame  $t$  is smaller than 7 pixels (23  $\mu\text{m}$ ), the algorithm calculates the combined centroid (figure 2.5b):

$$\mathbf{C}_{jk} = \frac{\mathbf{C}_j A_j + \mathbf{C}_k A_k}{A_j + A_k} \quad (2.1)$$

Particles  $j$  and  $k$  are merged or split, if the difference between calculated aggregate centroid  $\mathbf{C}_{jk}$  in frame  $t$  and actual particle centroid  $\mathbf{C}_l$  in frame  $t + i$  is smaller than 30 pixels (97  $\mu\text{m}$ ).

### 2.3.3 Track classification

The extracted tracks were subsequently validated and grouped into five classes: single filaments, interacting or ghosting (non-interacting) filament pairs, multiple filament aggregates and noise. The presented classification parameters were guessed based on observations.

Assuming that intermittent tracks were noise, we discarded tracks with an intermittency higher than 30 %:

$$\frac{f_{i,end} - f_{i,start}}{n_i} < 1.3 \quad (2.2)$$

where  $f_{i,start}$  and  $f_{i,end}$  are the starting and ending frame numbers and  $n_i$  is the total number of frames containing track  $i$ .

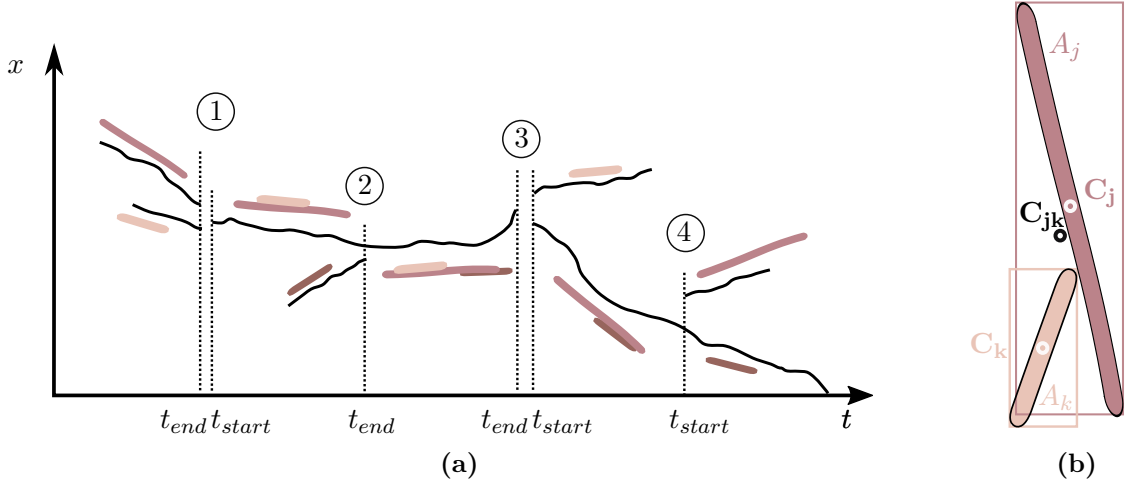


**Figure 2.5:** Merging and splitting of track segments. (a) Merging and splitting events: (1) two track ends are linked to one track start, (2) one track end is linked to the track middle of another track, (3) one track end is linked to two track starts and (4) one track start is linked to the track middle of another track. The continuous tracks in (2) and (4) are split into a single filament and aggregate track [27]. (b) Calculation of estimated aggregate centroid  $\mathbf{C}_{jk}$  of particles  $j$  and  $k$ .

Single filament tracks were selected based on eccentricity and length variation. The eccentricity describes the shape of a particle, i.e. the eccentricity of a circle is zero and the eccentricity of a single filament is generally between 0.9 and 1. Specifically, tracks were classified as single filament tracks if they were labeled as aggregate track (section 2.3.2) and fulfilled one of the following conditions:

$$\{\bar{e}_i > 0.98 \wedge c_{v,length,i} < 0.06\} \quad \text{or} \quad \{\bar{e}_i > 0.93 \wedge c_{v,length,i} < 0.02\} \quad (2.3)$$

where  $\bar{e}_i$  is the track averaged eccentricity and  $c_{v,length,i}$  is the coefficient of variation of particle length. Two different conditions were considered because shorter filaments have on average lower eccentricity.

Aggregate tracks were classified as filament pair tracks if both tracks that merged to form the filament pair or split from the pair were single filament tracks. If the mean ratio of eigenvalues was smaller than 0.02, the filament interaction was labeled as gliding or twisting, otherwise as ghosting interaction (cf. section 3.1.1).

Aggregate tracks that were not classified as filament pair tracks were labeled multiple filament aggregates. Similarly, tracks which were not labeled as single filament or aggregate track were classified as noise.

### 2.3.4 Performance

The tracking results were evaluated qualitatively by randomly checking particle tracks. The median background segmentation was very reliable and did not generate much noise. Particles and track segments were successfully linked; no wrong links and only few missing links have been detected. The merging and splitting algorithm was biased to detect short aggregate interactions, since it failed to capture filament pairs that split from a bigger bundle to merge with another aggregate track. Since there was no time to further improve the merging and splitting algorithm, all interacting filament pair tracks were checked and, if needed, added manually. The classification of ghosting

interactions was not checked, because this type of interaction characteristically has a shorter track duration and is therefore well captured by the merging and splitting algorithm.

## 2.4 Segmentation of filament pairs

Tracks of filament pair were further processed to separate the single filaments and to quantify their motion relative to each other. The segmentation was based on a combination of distance and intensity thresholding, given that filaments were either overlapping vertically or horizontally, i.e. they were positioned next or on top of each other (cf. figure 2.6b). The processing pipeline follows the steps shown in figure 2.6a.

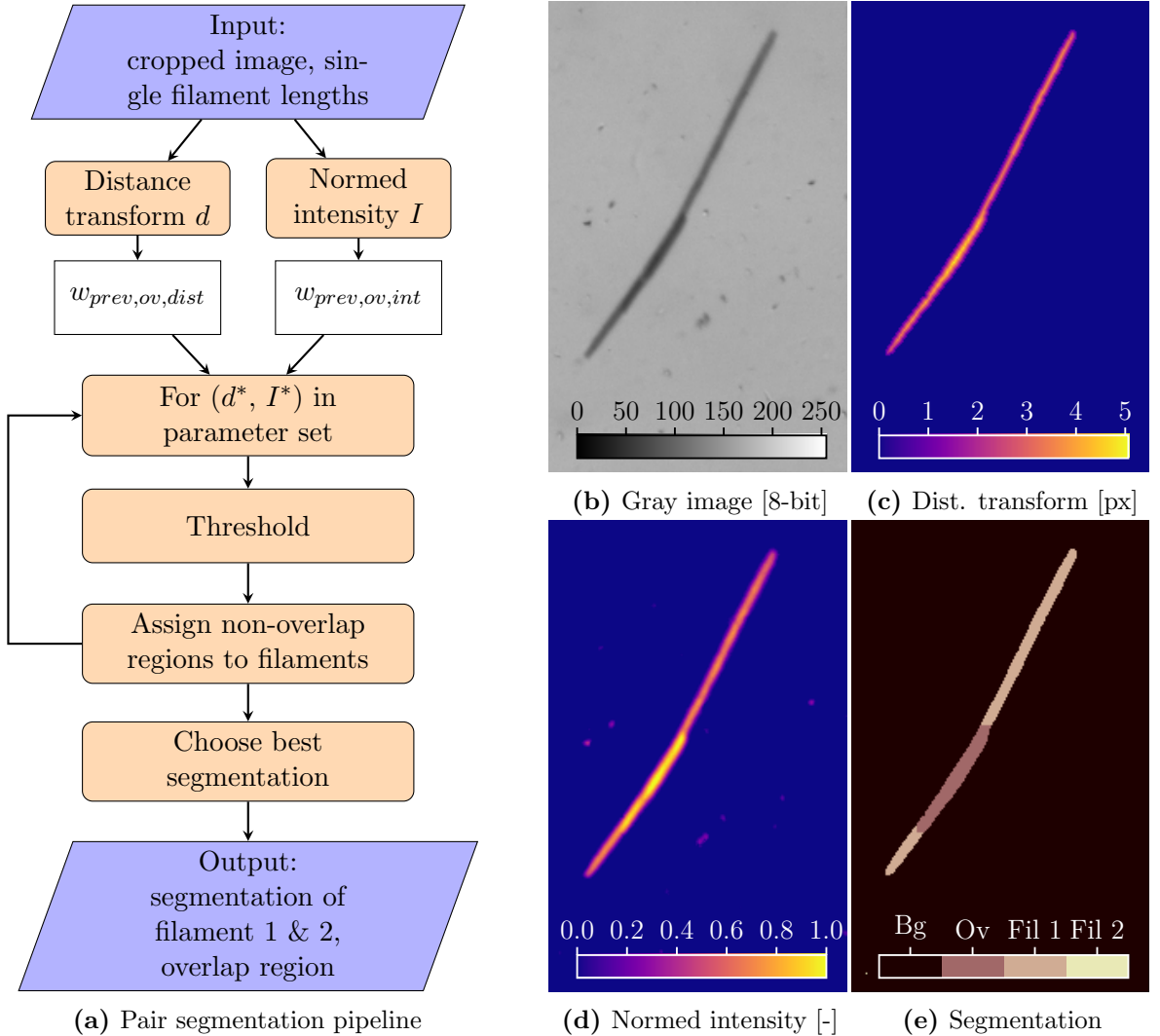


**Figure 2.6:** Segmentation of overlap region based on distance and intensity thresholding. (a) Processing pipeline with weighting functions  $w_{prev,ov}$  of overlap region in previous time step. (b)-(d) Example images of processing pipeline. (e) Segmented image with background (Bg), overlap region (Ov), filament 1 (Fil 1) and filament 2 (Fil 2)

### 2.4.1 Distance transform

The distance transform  $d$  calculates the Euclidean distance of a pixel within an object to the closest boundary pixel and is therefore suited to flag adjoining filaments (figure 2.6c). For single filaments,  $d$  ranged consistently between 2 to 3 pixels, for filament pairs situated side-by-side between 4 to 5 pixels. The transform  $d$  was calculated using the OpenCV `distanceTransform` function [25].

### 2.4.2 Normed intensity

Vertically stacked filament pairs are more effectively separated by intensity thresholding (figure 2.6d). The normed intensity was calculated as

$$I = \frac{I_{fg} - Q_{I_{fg},0.01}}{Q_{I_{fg},0.99} - Q_{I_{fg},0.01}} \quad (2.4)$$

where  $I_{fg}$  denotes the foreground intensity, which is the smoothed gray image ( $5 \times 5$  Gaussian blur) minus the background, and  $Q_{I_{fg},i}$  is the  $i^{\text{th}}$  quantile within the object.

### 2.4.3 Previous overlap weighting

Since filaments moved relatively slowly between subsequent frames, the distance transform  $d$  and normed intensity  $I$  were weighted with a function of the previous overlap region to improve segmentation. The weighting function  $w_{\text{prev,ov},d}$  of the distance transform  $d$  is heuristically defined as

$$w_{\text{prev,ov},d} = \begin{cases} (40 - r_{\text{prev,ov}})/40 & \text{if } r_{\text{prev,ov}} < 40 \\ 0 & \text{if } r_{\text{prev,ov}} > 40 \end{cases} \quad (2.5)$$

where  $r_{\text{prev,ov}}$  denotes the inverse distance transform from a background pixel to the boundary of the foreground object, here the overlap region of the previous frame. Similarly, the intensity weighting function  $w_{\text{prev,ov},I}$  is defined as

$$w_{\text{prev,ov},I} = \begin{cases} (15 - r_{\text{prev,ov}})^2/15 & \text{if } r_{\text{prev,ov}} < 15 \\ 0 & \text{if } r_{\text{prev,ov}} > 15 \end{cases} \quad (2.6)$$

### 2.4.4 Distance and intensity threshold parameters

Depending on the relative positions of filaments, different threshold parameters for  $d$  and  $I$  separated the filament pair more effectively. Therefore, the filament pair was segmented for different threshold parameters  $d^*$  and  $I^*$  out of a given parameter set and the best, cost-minimizing segmentation was subsequently chosen. The parameters were optimized on a finite option set because segmentation results were not sensitive on exact threshold values and for performance reasons.

Five parameter sets of  $d$  and  $I$  were heuristically obtained to cover different lighting conditions and were provided as input:

- $\{d > 4.0\}$
- $\{d > 4.0\}$  or  $\{d > 3.0 \wedge I > 0.70\}$
- $\{d > 4.0\}$  or  $\{d > 3.0 \wedge I > 0.85\}$
- $\{d > 4.0\}$  or  $\{d > 3.0 \wedge I > 0.70\}$  or  $\{d > 2.8 \wedge I > 0.80\}$
- $\{d > 4.0\}$  or  $\{d > 2.6 \wedge I > 0.55\}$  or  $\{d > 2.0 \wedge I > 0.65\}$

The cost  $c$  was defined as difference of input and segmented single filament length

$$c = ((l_1 - l_{1,in})^2 + (l_2 - l_{2,in})^2)^{0.5} \quad (2.7)$$

where  $l_i$  is the length of filament  $i$  in the segmented image of the current frame and  $l_{i,avg}$  is the input filament length (from merging and splitting algorithm in section 2.3.2).

If the cost exceeded 40 pixels, the segmentation was discarded and a Nan-value was entered in the overlap time series.

#### 2.4.5 Overlap region

The topological skeleton of the overlap region was retrieved by combining the thresholding results of  $d$  and  $I$  with thresholds  $(d^*, I^*)$ . The entire overlap region (as in figure 2.6e) was determined by dilating the retrieved skeleton, connecting different regions and clipping the region with object foreground.

#### 2.4.6 Allocation of non-overlap region to filaments

The steps described above identified the region where the two filaments are overlapping. In a further step, the remaining regions, i.e. non-overlapping regions, were allocated to a specific single filament (figure 2.6e). From just looking at the gray image in figure 2.6b, it is impossible to determine if the smaller filament is completely overlapping with the longer filament or if it extends further. The allocation was therefore based on previous information of segmentation or based on average filament lengths difference. Non-overlap regions were linked to regions in the previous frame with the linking algorithm described in section 2.3.2 up to a maximal radius of 5 pixels. If they could not be linked, the ends were assigned to best match input filament lengths considering geometric relations.

#### 2.4.7 Performance

The filament pair segmentation was evaluated based on the time series of the segmented filament lengths. Over all tracks, an average of 2.9 % frames were discarded because the segmentation cost exceeded 40 pixels (cf. section 2.4.4). In most cases, it was impossible to separate the filament pair manually, because the filaments were twisted and the overlapping region could not be identified. The average coefficient of variation  $c_{v,length}$  of filament length was 0.03, which is close to the  $c_{v,length}$  parameters used for single filament classification in section 2.3.3.

## 2.5 Calculation of derived quantities

### 2.5.1 Measures of overlap

Based on the segmented filament pair sequence (section 2.4), lack of overlap ( $LOL$ ) and position ( $Pos$ ) were calculated to characterize the filament pair interaction (figure 2.7).  $LOL$  is defined as the fraction of the shorter filament which is not overlapping with the longer filament. The definition is based on the shorter filament, given that the longer filament is extending further than the shorter filament.  $Pos$  is the projection of the centroid position of the short filament on the long filament.

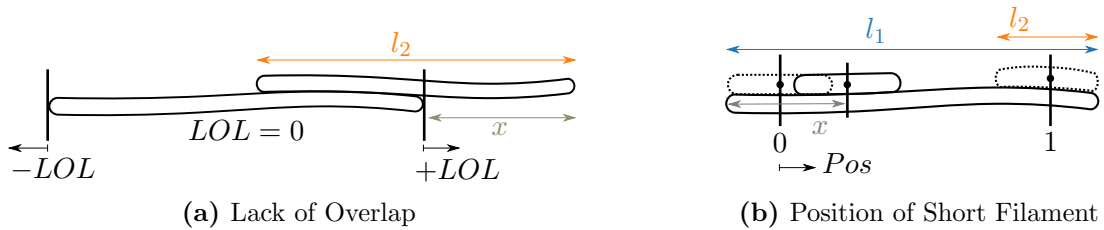


**Figure 2.7:** Characteristic measures of overlap.

### 2.5.2 Velocity

The absolute single filament velocity was calculated from the trajectory of centroid position, which was smoothed with a centered moving average (MA) filter of window size 7. The velocity was further smoothed with a MA-filter of size 5. The direction of the movement was defined as positive and accordingly negative, if the filament moved to the East or to the West, respectively.

For filament pairs, the relative filament velocity was defined as difference in smoothed position  $Pos$  (MA of size 5) between consecutive time steps.

### 2.5.3 Reversal frequency

The overall reversal frequency is the number of reversals  $n_{rev}$  divided by the track length  $t$  of all tracks as defined in equation 2.8.

$$f_{rev} = \frac{\sum_i n_{rev,i}}{\sum_i t_i} \quad (2.8)$$

A single filament reversal was defined as a zero-crossing of instantaneous velocity which exceeded  $\pm 0.1 \mu\text{m s}^{-1}$  (figure 2.8a). If filament velocity was smaller than  $0.1 \mu\text{m s}^{-1}$ , the filament was stagnant and zero-crossings were not considered, due to noise fluctuations.

A filament pair reversal was defined as peak in  $Pos$  (figure 2.8b). The peaks were calculated with the function `scipy.signal.find_peaks` [28] with the minimal prominence set to  $20 \mu\text{m}$ , which is approximately 2 to 3 individual cells.

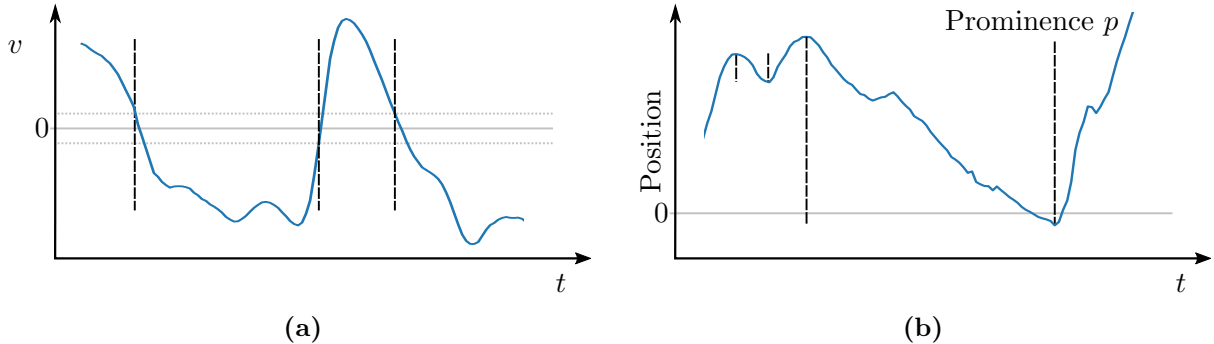


**Figure 2.8:** Definition of reversals for single filaments (a) and filament pairs (b). The dashed vertical lines indicate identified reversals in (a) and (b) as well as prominence height in (b). The dotted horizontal lines in (a) illustrate the band of  $\pm 0.1 \mu\text{m s}^{-1}$  velocity.

## 2.6 Statistics

### 2.6.1 Parameter estimation

It was assumed that interaction times followed an exponential distribution with mean duration of interaction  $t_{pair}$  and ending rate  $\lambda_{pair}$ . The parameters were calculated with maximum likelihood estimation

$$\lambda_{pair} = \frac{1}{t_{pair}} = \frac{n}{\sum t_i} \quad (2.9)$$

where  $t_i$  is the track time of observation  $i$  and  $n$  is the total number of observations.

### 2.6.2 Statistical test

The Wilcoxon-Mann-Whitney two-sample rank-sum test, or Mann-Whitney- $U$ -test, was used to test if distributions between aggregating and non-aggregating cultures were statistically different [29]. Specifically, it was tested if the relative filament velocity was lower and the interaction time was higher for the aggregating culture samples using the Python implementation `scipy.stats.mannwhitneyu` [28]. A significance value of 1% was chosen.

# 3 Results

## 3.1 Types of filament pair interactions

Filament pair interactions differed in the type of relative movement, the number of reversals and the relative filament velocity, which in turn influenced the duration of interaction.

### 3.1.1 Types of relative movement

We observed three main types of relative movements: gliding, twisting and ghosting (Figure 3.1). Gliding or twisting movements were characterized by the filaments gliding parallel or helical along each other. The movement of an interacting filament pair generally alternated between gliding and twisting. Filaments in ghosting interaction did not interact with the other filament, but crossed the other filament at the given meeting angle. Filaments meeting at a perpendicular angle did mostly not align, but alignment is theoretically possible and was occasionally observed.

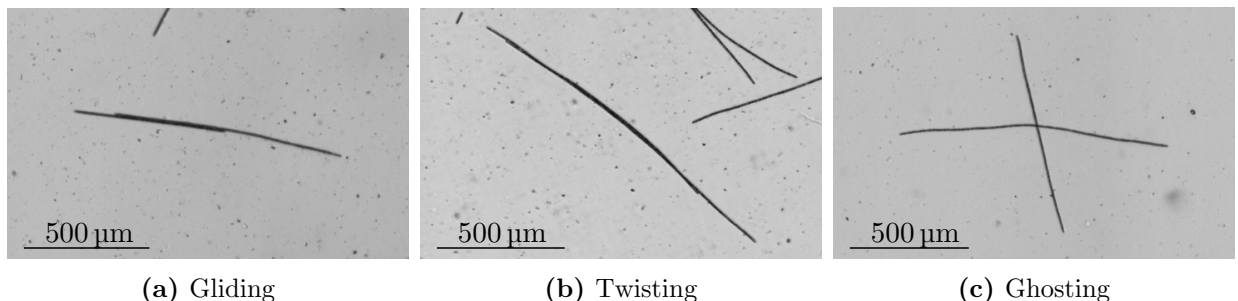


**Figure 3.1:** Types of relative movements in filament pair interactions

About 20 % of recorded filament pairs interacted by gliding on the other filament. No difference between aggregating and non-aggregating cultures was observed (table 3.1). Ghosting interactions were excluded from the subsequent analyses.

**Table 3.1:** Fraction of relative movement types in aggregating and non-aggregating cultures.

	Gliding / Twisting	Ghosting
Aggregating ( $n = 1197$ )	20.97 %	79.03 %
Non-Aggregating ( $n = 1278$ )	21.67 %	78.33 %

### 3.1.2 Endings of filament pair tracks

Filament pair tracks ended because of five reasons: (1) the filament pair merged with a third filament or filament bundle, (2) the pair separated, (3) the experiment ended, (4) the pair glided outside the field of view or (5) the track ended due to noise in the image analysis pipeline. Irrespective of the physiological state of the culture, only about 30 % of filament pair tracks ended by separation of the filaments (figure 3.2).

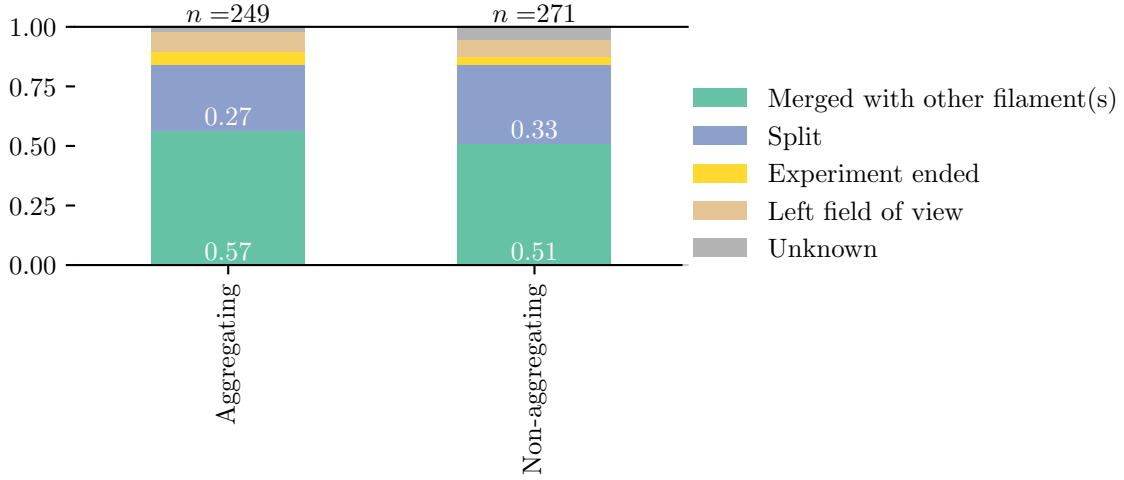


**Figure 3.2:** Filament pair track endings in aggregating and non-aggregating cultures.

Reasons (2) to (5), in the following referred to as "no separation", terminate the recording of pair interactions prematurely. The interaction time is thus systematically underestimated in 70 % of the cases. Nevertheless, all filament pair tracks are included in the subsequent analyses, since the fraction of pairs that do not separate is similar in the aggregating and non-aggregating cultures (figure 3.2). Despite the underestimation of interaction time, non-separating tracks are on average 30 % longer than separating tracks (figure 3.3b).

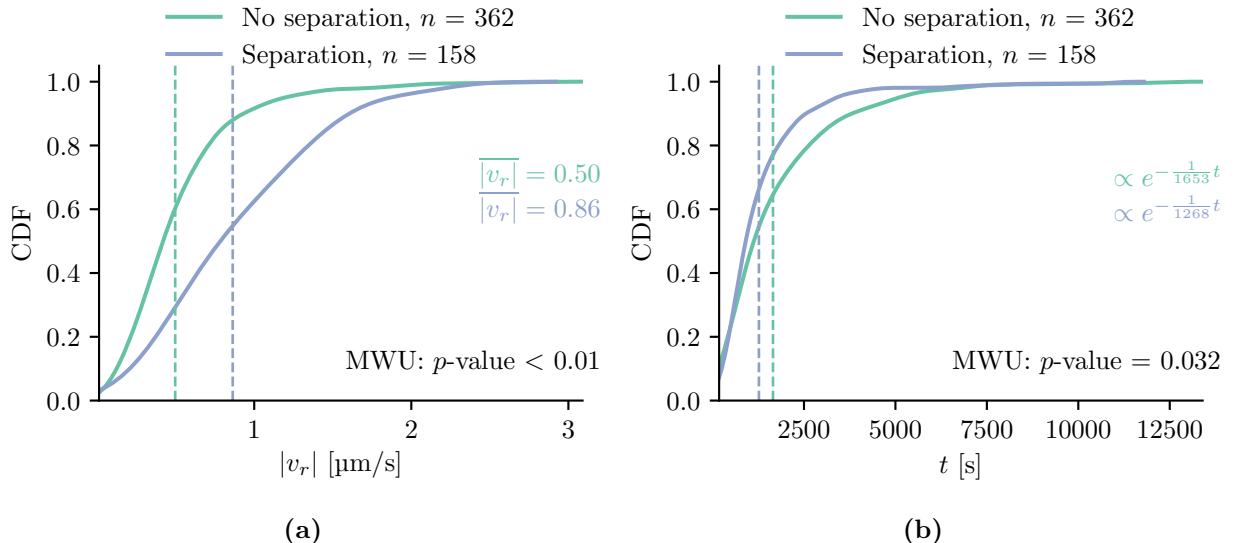


**Figure 3.3:** CDF of (a) absolute value of relative filament velocity and (b) interaction time of non-separating and separating tracks. Mean values are indicated with dashed horizontal lines. Fitted distributions and  $p$ -values of the Mann-Whitney- $U$ -test (MWU) are shown on the left.

Separating pairs have significantly higher relative velocity than non-separating pairs (figure 3.3a). In fact, the fraction of separating pairs rises from 10 % to 80 % for velocities between 0 to  $1 \mu\text{m s}^{-1}$  in aggregating cultures, but stays constant around 35 % in non-aggregating cultures (figures 3.4a and 3.4b). In non-aggregating cultures, the fraction of separating pairs increases to about 90 % between 1 to  $1.5 \mu\text{m s}^{-1}$ .

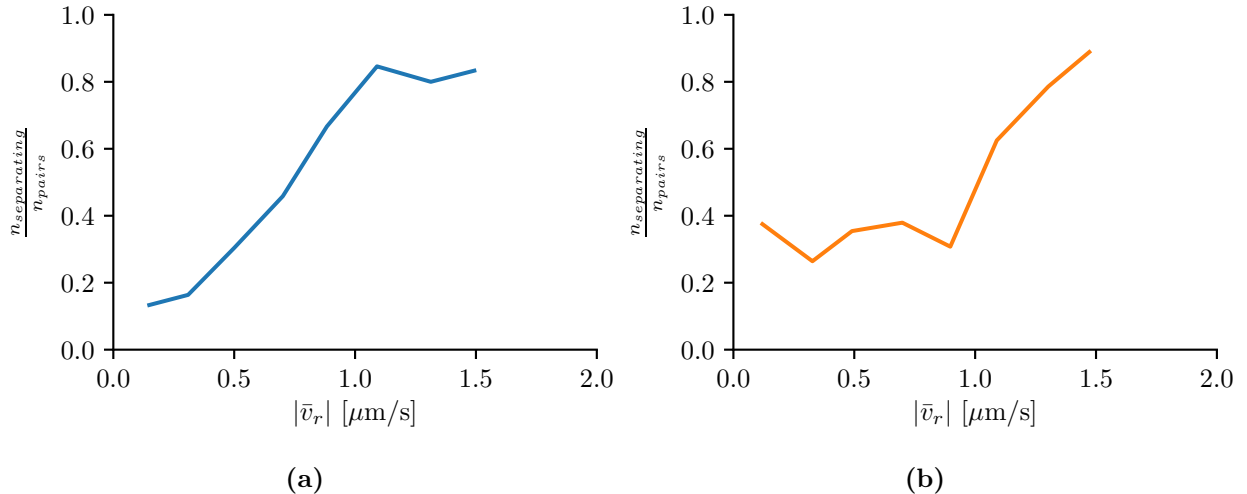


**Figure 3.4:** Fraction of separating pairs as function of track averaged relative filament velocity in (a) aggregating and (b) non-aggregating cultures. The fraction was calculated for  $v_r$  bins of  $0.2 \mu\text{m s}^{-1}$  width. Bins with less than four observation are not shown. Non-reversing and non-separating filament pairs were excluded from the calculation (cf. section 3.1.3).

### 3.1.3 Reversing and non-reversing pairs

The duration of filament pair interactions varied considerably. Some pairs moved periodically along each other and reversed at a characteristic *LOL*. Others did not reverse and naturally separated by gliding apart.

In both aggregating and non-aggregating cultures, about 60 % of all filament pairs reversed at least once (figure 3.5). The fraction of reversing pairs that separated was slightly higher in the non-aggregating culture. The fraction of non-reversing, separating pairs was about 15 %.

Tracks of filament pairs that did neither reverse nor separate were typically quite short (cf. figure D.2d in appendix D). The filament pairs encountered a third filament before the pair had a chance to reverse or separate.

The interaction time is on average about 4 times greater for reversing than for non-reversing pairs (figure 3.6a). The maximum interaction time even increases sixfold from 2000 s to 12 000 s. The overlap velocity is 1.3 times higher for non-reversing pairs (figure 3.6b).

The fraction of reversing pairs is a function of relative filament velocity: the reversing fraction peaks at 100 % around  $0.3$  or  $1 \mu\text{m s}^{-1}$  for aggregating and non-aggregating pairs, respectively (figure 3.7a and 3.7b). The fraction decreases to 20 to 30 % for velocities of  $1.5 \mu\text{m s}^{-1}$ .

The fraction of reversing pairs is also a function of total filament length and increases slightly with increasing total length (figure 3.8).

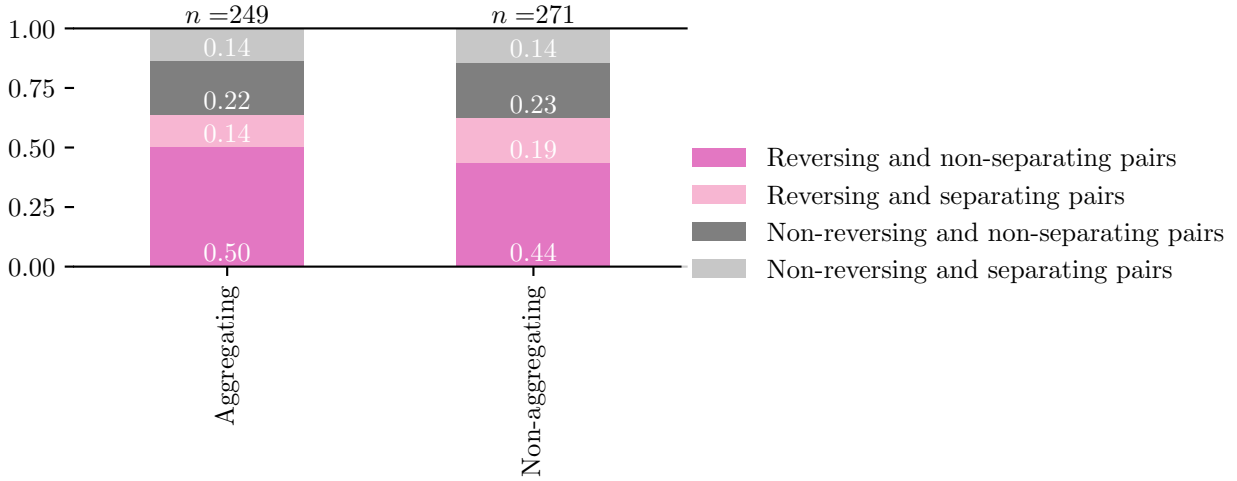


**Figure 3.5:** Fraction of reversing/non-reversing and separating/non-separating filament pair interactions in aggregating and non-aggregating cultures.

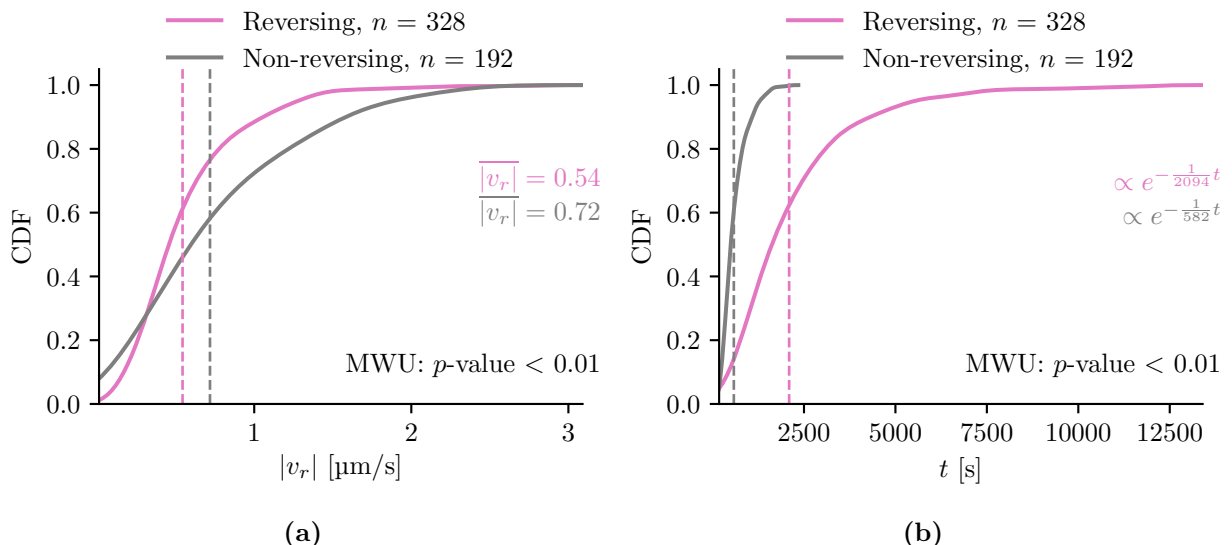


**Figure 3.6:** CDF of (a) absolute value of relative filament velocity and (b) interaction time of reversing and non-reversing tracks. Mean values are indicated with dashed horizontal lines. Fitted distributions and  $p$ -values of the Mann-Whitney- $U$ -test (MWU) are shown on the left.

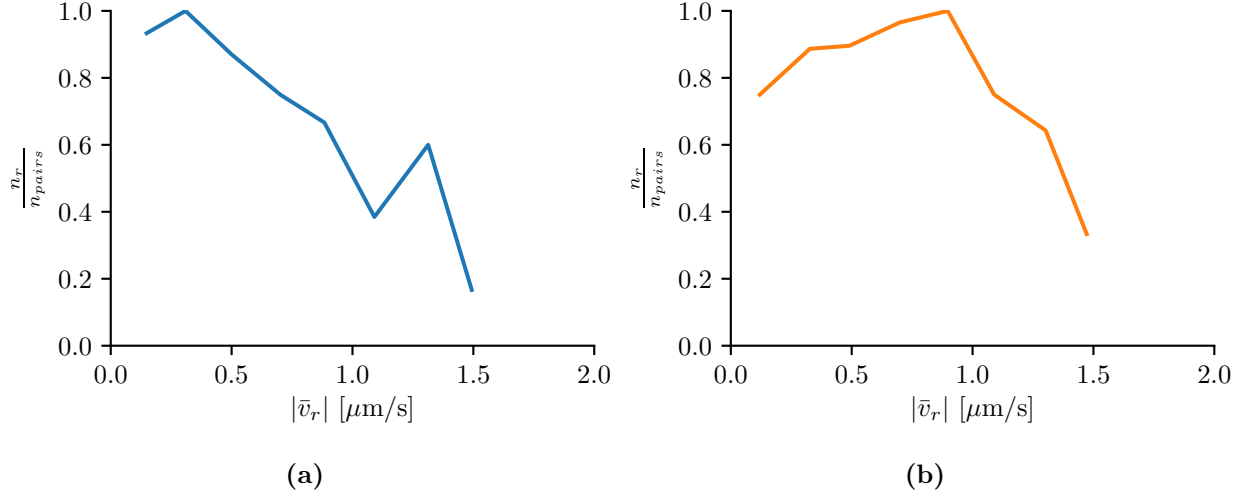


**Figure 3.7:** Fraction of reversing pairs as function of track averaged relative filament velocity in (a) aggregating and (b) non-aggregating cultures. The fraction was averaged for  $v_r$  bins of  $0.2 \mu\text{m s}^{-1}$  width. Bins with less than four observation are not shown. Non-reversing and non-separating filament pairs were excluded from the calculation (cf. section 3.1.3).

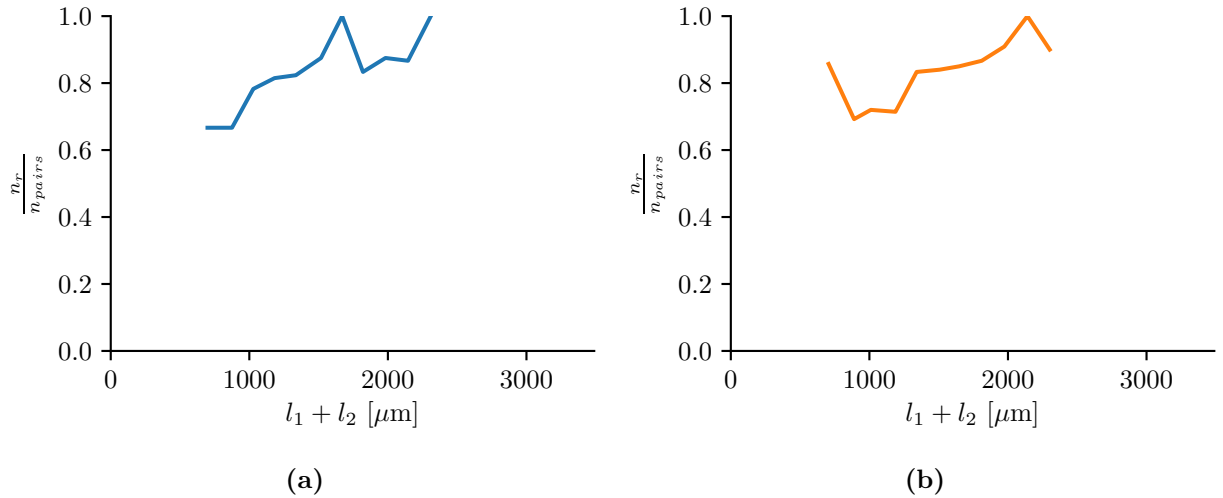


**Figure 3.8:** Fraction of reversing pairs as function of summed filament lengths in (a) aggregating and (b) non-aggregating cultures. The fraction was averaged for  $l_1 + l_2$  bins of  $160 \mu\text{m}$  width. Bins with less than four observation are not shown. Non-reversing and non-separating filament pairs were excluded from the calculation (cf. section 3.1.3)

## 3.2 Kinetics of filament pair interactions

### 3.2.1 Relative filament velocity

Single filaments of the non-aggregating culture glide on average 1.24 times faster than filaments of aggregating culture sample (figure 3.9a). Similarly, pairs in non-aggregating cultures have a 22 % higher average relative velocity (figure 3.9b). The *LOL*-velocity  $v_{LOL}$ , which is positive if absolute  $|LOL|$  is increasing and negative if it is decreasing, is mostly constant for different  $LOL$  values (figure 3.10).

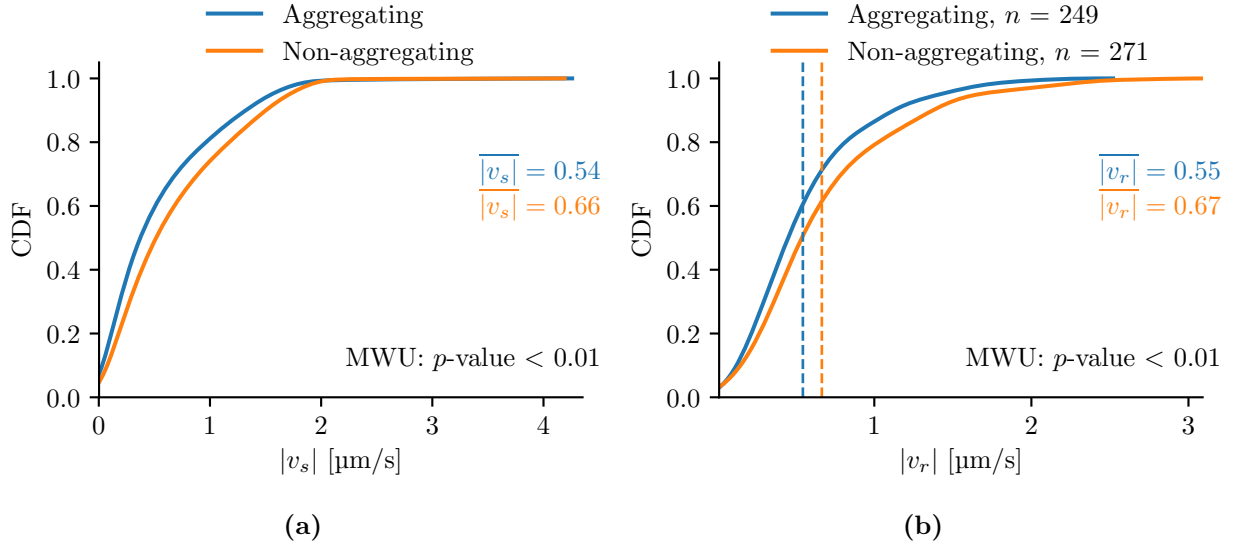


**Figure 3.9:** CDF of track averaged (a) absolute single filament velocity and (b) absolute value of relative filament velocity of filament pairs comparing aggregating and non-aggregating cultures. Mean values are indicated with dashed horizontal lines. Fitted distributions and  $p$ -values of the Mann-Whitney- $U$ -test (MWU) are shown on the left.

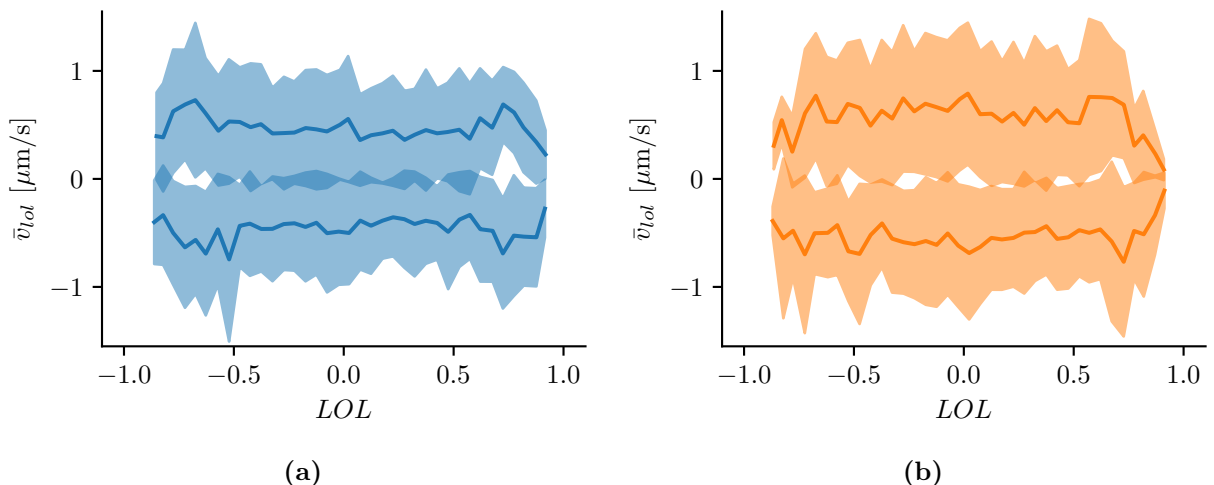


**Figure 3.10:** Smoothed, instantaneous *LOL* velocity  $v_{LOL}$  (mean  $\pm$  std) as function of *LOL* in (a) aggregating and (b) non-aggregating cultures.  $v_{LOL}$  is defined positive or negative, if absolute  $|LOL|$  is increasing or decreasing, respectively. The overlap velocity was averaged for *LOL* bins of 0.2 width. Bins with less than four observation are not shown.

### 3.2.2 Reversal statistics

#### Mean reversal frequency

Filament pairs reverse more frequently than single trichomes: an average filament pair reverses every 12 minutes, whereas a single filament reverses every 35 to 44 minutes (table 3.2). The physiological state of the culture, i.e. aggregating or non-aggregating, only slightly affects  $f_{rev}$ . Filaments in non-aggregating cultures reverse more often, but cover a greater distance between reversals. The mean distances between pair reversals in aggregating and non-aggregating culture samples correspond to about half and two thirds of mean filament length, respectively.

**Table 3.2:** Mean reversal frequency  $f_{rev}$  and mean reversal distance  $d_{rev}$  of single filaments and filament pairs in aggregating (Agg.) and non-aggregating (NAgg.) cultures.

	$f_{rev}$ [s <sup>-1</sup> ]		$d_{rev}$ [\mu m]	
	Agg.	NAgg.	Agg.	NAgg.
Single Filaments	$3.71 \times 10^{-4}$	$4.69 \times 10^{-4}$	1443	1412
Filament Pairs	$1.44 \times 10^{-3}$	$1.46 \times 10^{-3}$	377	457

#### Total Filament Pair Gliding Distance

The total normed gliding distance is defined as the total distance a filament pair glides along each other  $d_{glide}$  divided by the total filament length and approximates the number of reversals per track independent of filament length. The gliding distance is naturally higher for reversing pairs (cf. figures 3.11a and 3.11b). It is only slightly and not significantly higher for aggregating than for non-aggregating cultures.

#### LOL at Reversal Points

The lack of overlap at reversal points  $LOL_{rev}$  is similar for aggregating and non-aggregating cultures (figure 3.12). Non-separating filament pairs reverse at lower  $LOL_{rev}$  values than separating pairs (one-sided MWU-test,  $p$ -value < 0.01). The mean  $LOL_{rev}$  is 0.22 and 0.28 for non-separating and separating filament pairs, respectively. Taking the average filament length of 700 \mu m, the difference in average  $LOL_{rev}$  corresponds to 6 cells out of 100 cells per filament.

Different normalization of overlap and non-overlap lengths at reversal points are shown in appendix B. Specifically, no difference between aggregating and non-aggregating cultures was found for the following measures: absolute non-overlap length of shorter filament ( $x_{LOL}$ ) (figure B.1), non-overlap length of the shorter filament normalized by total filament pair length ( $x_{LOL}/(l_1 + l_2 - l_{ov})$ ) (figure B.2a), non-overlap length of the shorter filament normalized by summed filament pair length ( $x_{LOL}/(l_1 + l_2)$ ) (figure B.2b), overlap length ( $l_{ov}$ ) (figure B.3a), overlap length normalized by shorter filament length ( $l_{ov}/l_2$ ) (figure B.3b).

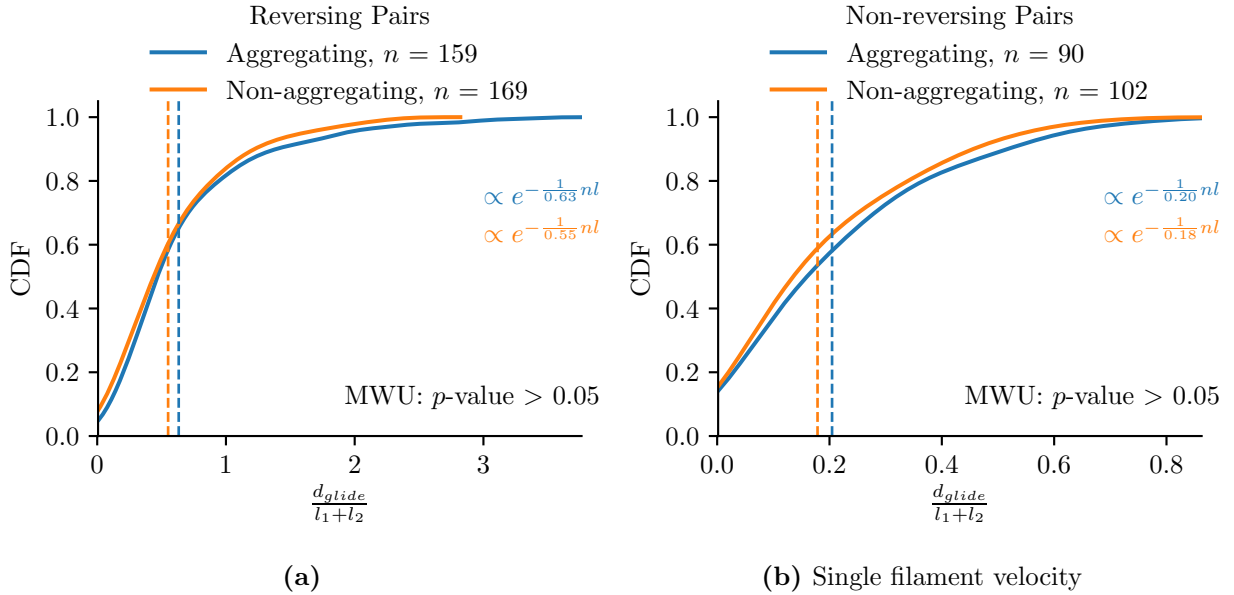


**Figure 3.11:** CDF of normed total gliding distance in (a) reversing and (b) non-reversing pairs comparing aggregating and non-aggregating cultures. Mean values are indicated with dashed horizontal lines. Fitted distributions and  $p$ -values of the Mann-Whitney- $U$ -test (MWU) are shown on the left.

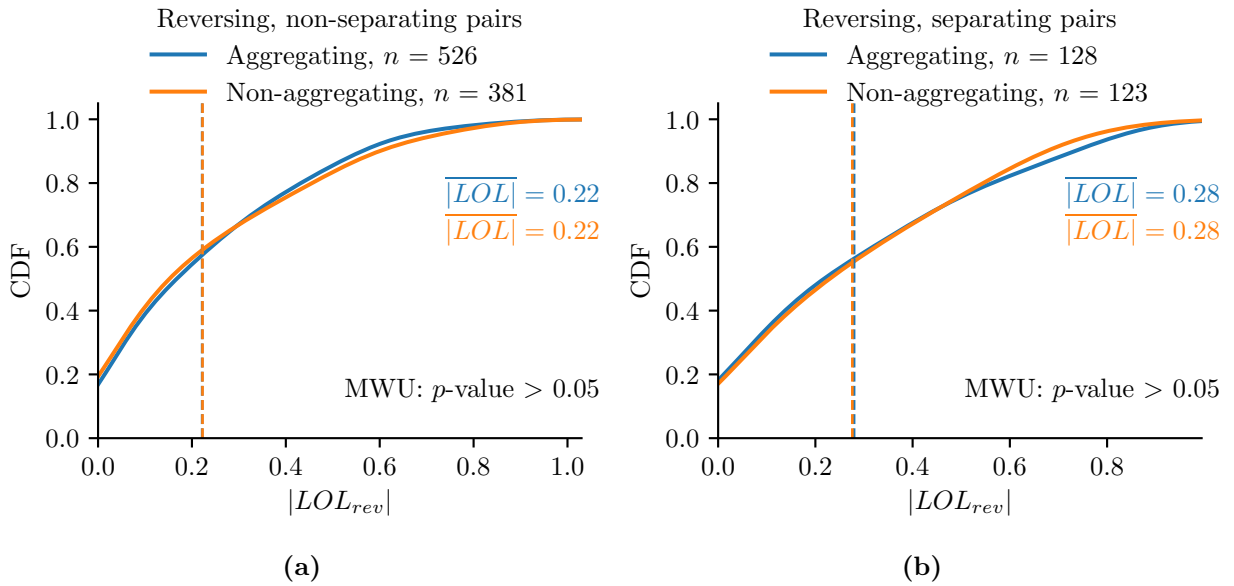


**Figure 3.12:** CDF of  $LOL$  at reversal points of (a) non-separating and (b) separating filament pairs comparing aggregating and non-aggregating cultures. Mean values are indicated with dashed horizontal lines. Fitted distributions and  $p$ -values of the Mann-Whitney- $U$ -test (MWU) are shown on the left.

### 3.3 Interaction time

The interaction time of a filament pair is defined as the duration the two filaments are identified as one single particle during particle tracking (section 2.3.1). This includes the alignment time in the beginning of the interaction. Filament pairs that separated from a larger bundle were also included in the analysis, the track time starts the moment the pair is distinguished as single particle. As seen in section 3.1.3, interaction time is mostly affected by the presence of reversals.

An overview of average interaction time and overlap velocity for different subgroups of filament pairs is shown in table 3.3. The corresponding distributions are displayed in appendix D.

The duration of single filament tracks is 1.24 times higher in aggregating cultures, which corresponds to the 1.24 times higher filament velocity. The higher velocity increases the probability of track end by encountering another filament or gliding outside the field of view. The interaction time of all filament pairs irrespective of track ending is 43 % longer in aggregating than non-aggregating cultures (figure 3.13b).

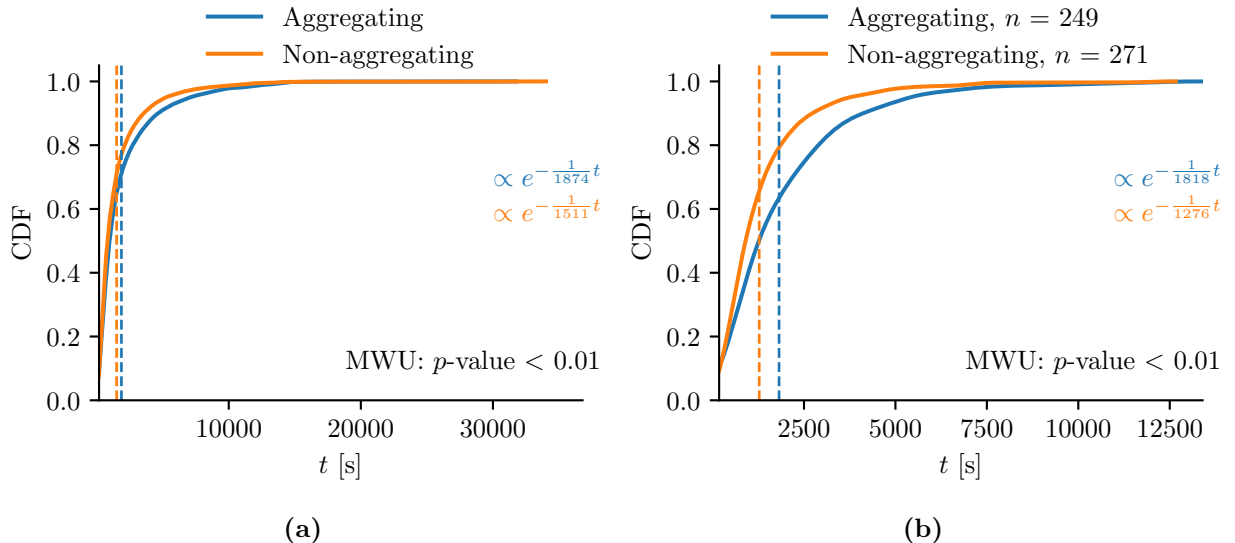


**Figure 3.13:** CDF of filament interaction times  $t$  of (a) single filaments and (b) filament pairs comparing aggregating and non-aggregating cultures. Mean values are indicated with dashed horizontal lines. Fitted distributions and  $p$ -values of the Mann-Whitney- $U$ -test (MWU) are shown on the left.

The interaction time of reversing pairs is 46 % longer in aggregating than non-aggregating cultures. The greatest increase of 61 % is observed for reversing, separating pairs, the increase is however not statistically significant because of the low number of observations (figure D.1d). The interaction time of non-reversing pairs are independent of the physiological state of the culture (figure D.2b).

**Table 3.3:** Mean track duration  $t$ , mean velocity  $v$  and the relative difference between cultures (as fraction of the lower value) for different subgroups in aggregating (Agg.) and non-aggregating (NAgg.) cultures. For single filaments the single filament velocity is shown, for filament pairs the relative filament velocity.

	$t$ [s]			$v$ [ $\mu\text{m}/\text{s}$ ]		
	Agg.	NAgg.	[-]	Agg.	NAgg.	[-]
Single filaments	1874	1511	1.24	0.54	0.66	1.24
Filament pairs	1818	1276	1.43	0.55	0.67	1.22
Reversing pairs	2503	1710	1.46	0.47	0.61	1.29
Non-reversing pairs	609	558	1.09	0.67	0.76	1.12
Separating pairs	1496	1094	1.37	0.82	0.89	1.09
Non-separating pairs	1939	1366	1.42	0.44	0.55	1.25
Reversing, non-separating pairs	2546	1821	1.40	0.42	0.54	1.31
Reversing, separating pairs	2343	1453	1.61	0.68	0.77	1.13
Non-reversing, non-separating pairs	584	516	1.13	0.50	0.57	1.15
Non-reversing, separating pairs	650	626	1.04	0.97	1.06	1.10

### 3.4 Effect of filament pair kinetics on interaction time

Filament pairs can increase their interaction time by reversing regularly, decreasing relative filament velocity or combining both approaches. Non-reversing and non-separating filament pairs are excluded from the subsequent analysis, as they do not provide any information on how interaction time is increased.

Unsurprisingly, the total gliding distance, as measure for reversal frequency, increases interaction time most substantially (figure 3.14). The interaction time is a function of  $d$  to the power of 0.63 for reversing pairs. Filament pairs in aggregating culture sample have longer interactions for the same gliding distance than pairs in non-aggregating cultures.

The stalling fraction is defined as the fraction of time the absolute value of relative filament velocity is smaller than  $0.1 \mu\text{m s}^{-1}$ .  $f_{\text{stalling}}$  does not directly affect the interaction time (figure 3.15). The straight lines in figure 3.15 are equal to  $1/(f_{\text{st}}t)$  and represent the limit of sampling, i.e. when the filament pair is only stalling in one to two frames.

The interaction time seems maximal at overlap velocities around  $0.3 \mu\text{m s}^{-1}$  as suggested by the 95 % quantile in figure 3.16. It is unresolved, if interaction times are indeed maximal because only few pairs are observed with average overlap velocities below  $0.3 \mu\text{m s}^{-1}$ . The decrease of interaction times with increasing overlap velocities coheres with the above results: filament pairs with higher overlap velocities have higher separation probability and therefore lower mean interaction times. Given the low number of observations at relative velocities greater than  $1 \mu\text{m s}^{-1}$ , the 95 % quantile is affected by outliers and thus peaks at  $1 \mu\text{m s}^{-1}$  (figure 3.16).

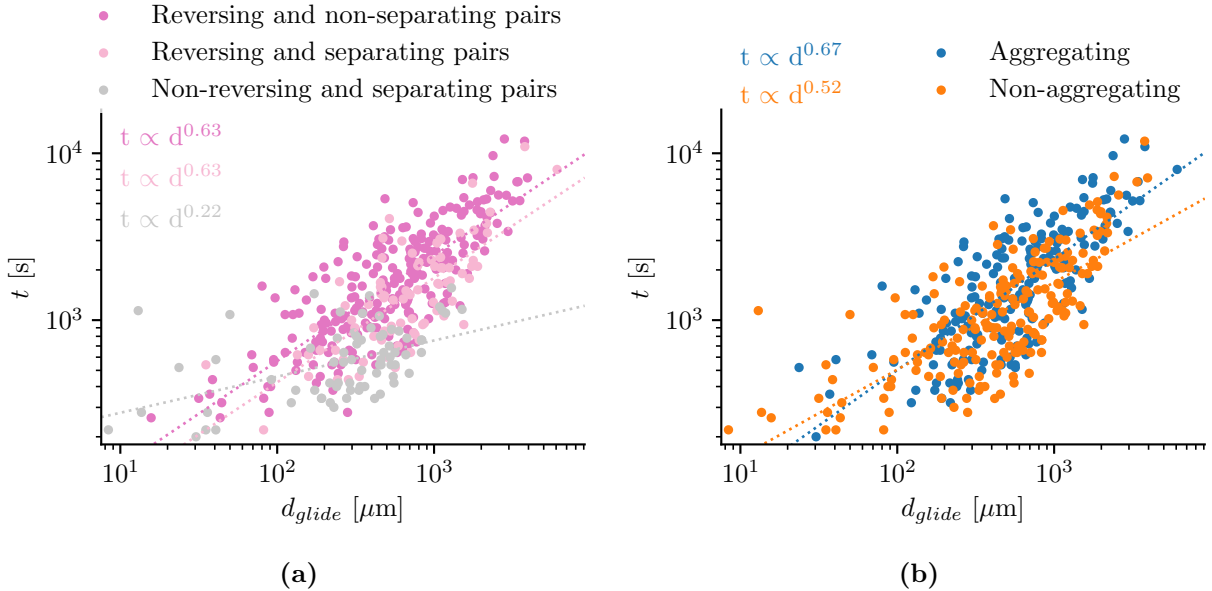


**Figure 3.14:** Effect of total relative gliding distance  $d_{glide}$  on filament pair interaction time. Non-reversing and non-separating filament pairs were excluded from the calculation (cf. section 3.1.3)

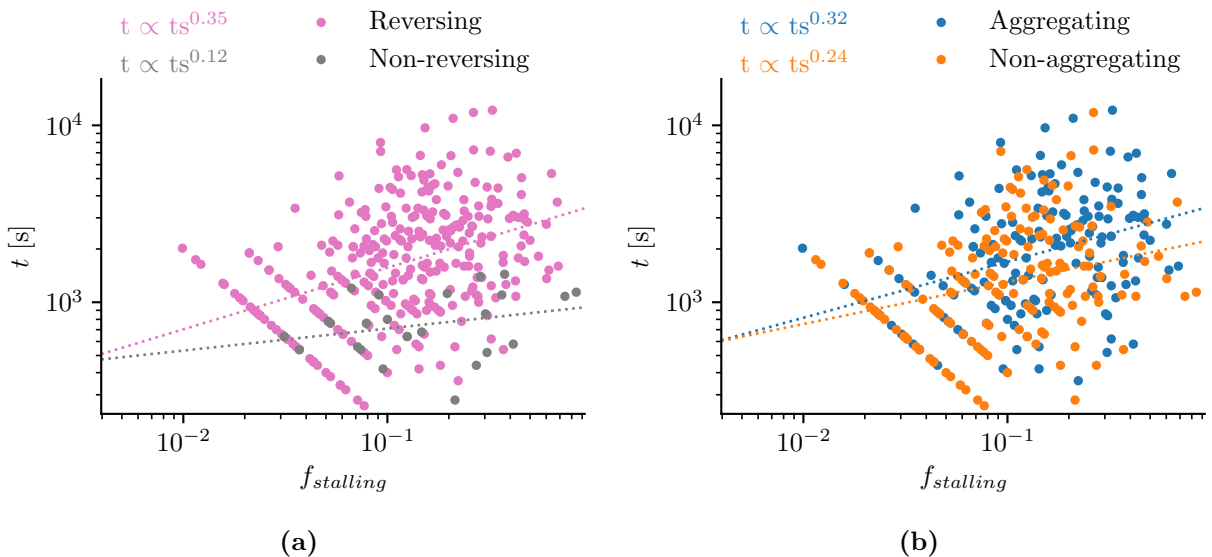


**Figure 3.15:** Effect of stalling time fraction  $f_{stalling}$  on filament pair interaction time. Non-reversing and non-separating filament pairs were excluded from the calculation (cf. section 3.1.3)

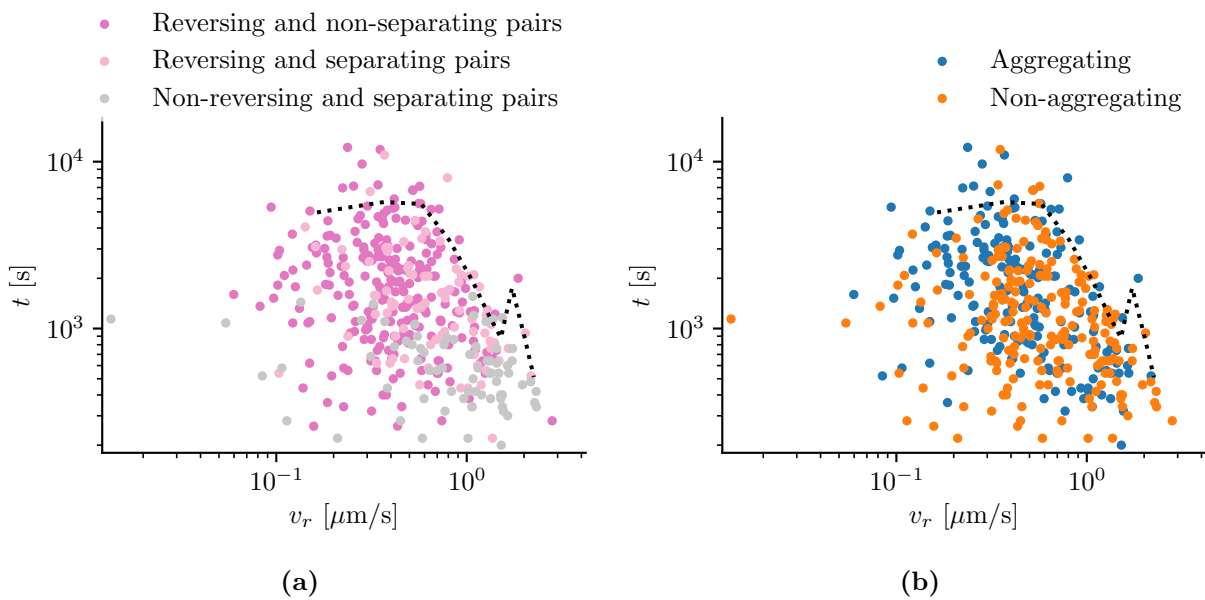


**Figure 3.16:** Effect of relative filament velocity  $v_r$  on filament pair interaction time. The 95 % quantile was calculated for  $v_r$  bins of  $0.15 \mu\text{m s}^{-1}$  width and is indicated with dotted lines. Non-reversing and non-separating filament pairs were excluded from the calculation (cf. section 3.1.3)

## 4 Discussion

### 4.1 Reversals

We found that *Trichodesmium* filament pairs effectively increase the duration of interaction by reversing more frequently than single filaments. Reversals are inherent to filament pair interactions independent of the physiological state of the culture. Reversals are deterministic and triggered by *LOL*. In consequence, trichomes reverse either actively by sensing change in *LOL* or passively by some restoring force associated with *LOL*.

Filament pairs reverse abruptly, i.e. they do not change the relative velocity with increasing *LOL*. This is unexpected seeing that in the viscous regime, velocity is proportional to the exerted gliding force. Gliding force is therefore not proportional to the relative contact area, but trichomes compensate the decrease in contact area by increasing force per area. Filaments might glide at a preferred gliding speed, which they can uphold over a range of conditions. However, filaments in the given experimental setup use both the second filament and the microscope slide as gliding substrate. The decrease in area is therefore only a small fraction of the total contact area. A free-floating filament pair might not be able to balance the relative velocity.

Although filament pair kinematics differ, the ratio of reversing to non-reversing pairs is constant between aggregating and non-aggregating cultures. This could suggest the existence of reversing and non-reversing subpopulations. However, no other indications support this suggestion and we did not further consider it.

### 4.2 Relative filament pair velocity

Relative filament velocity has two effects on interaction time: On one hand, the relative velocity determines the number of reversals necessary to remain attached for a certain duration. Therefore, assuming a constant separation probability per reversal, the separation probability is lower for reduced relative velocity. This decrease in probability is proportional to the mean difference in overlap velocity, i.e. filament pairs in aggregating cultures are expected to remain attached 30 % longer, as they are 30 % slower. On the other hand, relative filament velocity affects the separation probability per reversal. Filament pairs with a lower relative velocity are more likely to reverse and remain attached.

The fraction of reversing pairs drops drastically with increasing relative filament velocity. Potential explanations include two main mechanisms: (1) If reversals are only triggered after a certain signaling period, filament pairs might separate passively before the filaments have time to reverse. This is supported by a handful of observations of filaments reversing just after they separated and re-attaching to the other filament. Also, the fraction of reversing pairs increases with total filament pair length, which gives the filaments more time to reverse. (2) Faster filament pairs might actively separate because they are in a different physiological state, i.e. they are less stressed. The

fraction of separating pairs as a function of relative velocity differs between the aggregating and non-aggregating culture. This suggests that filament pairs can modulate the separation probability over a range of velocities. The two interpretations are not exclusive, but might complement each other. Stressed filaments might be on average slower and reverse more frequently because of longer signaling times.

### 4.3 Estimation of filament detachment rate

The time scales of different experiments with different filament densities have been combined for the analysis of pair interaction times, based on the assumption that filament pair separation depends on the physiological state of the culture and not on filament density. However, filament encounters are dependent on filament gliding velocity and filament density and in turn affect filament pair interaction times (assuming that separation time is greater than encounter time). For instance, in the extreme case that filament pairs never separate, the interaction time distribution would be governed by merging events. Assuming that the shape and absolute velocity of filament pairs are not considerably different from single trichomes, the distribution of pair interaction time and single filament track duration would hence converge. Equally, if only separating tracks are considered, the distribution of separation times is biased, i.e. underestimated, since the encounter times pose an upper limit to filament pair interactions.

As a first estimate of the unbiased separation times, the interaction time can be modeled as the combined Poisson process of filament encounters and filament pair separations, neglecting the small number of cases, in which tracks end due to other reasons (cf. figure 3.2 in section 3.1.2). The filament pair ending rate is then given as

$$\lambda_p = \lambda_m + \lambda_s \quad (4.1)$$

where  $\lambda_s$  is the mean encounter rate and  $\lambda_s$  the mean separation rate.

The fraction of merging and separation endings equals the ratio of rates (equation 4.2).

$$\frac{n_{merging}}{n_{pairs}} = \frac{\lambda_m}{\lambda_p} \quad \text{and} \quad \frac{n_{separating}}{n_{pairs}} = \frac{\lambda_s}{\lambda_p} \quad (4.2)$$

The distribution of interaction, merging and separation times roughly follow an exponential distribution, but have a slightly heavier tail. (figures E.1, E.2 and E.3, respectively, in appendix E).

Because of different encounter rates in experiments, the unbiased merging and separation times are first estimated for each experiment. Averaging over all experiments yields separation times of 9000 s and 4300 s in aggregating and non-aggregating cultures, respectively. Therefore, filament pairs remain attached about twice as long in the aggregating physiological state.

The similar distributions of interaction times of separating and non-separating pairs in section 3.1.2 could result from the effect of biased sampling. As simple test, sampling from the unbiased distributions  $Exp(\lambda_m)$  and  $Exp(\lambda_s)$  was simulated: A value was drawn from each distribution and the lower of both values was assigned to the corresponding set of realized values. The simulated distribution is quite similar to the observed distribution of interaction time for separating and non-separating filament pairs as shown in figure E.4 in appendix E.

The described approach is a first rough estimate of unbiased separation time. It could be improved by, for instance, including feedback of merging and separation events on the encounter rate. However, this is not within the scope of this project.

## 4.4 Can differences in filament pair interactions explain macroscopic aggregation?

Aggregate formation is generally expected if filament encounter rates are greater than detachment rates. Initial encounter times in the macroscopic setup are in the order of 3 minutes. In contrast, separation times are about 17 to 33 minutes, which is a factor of 8 to 9 greater than encounter rates for aggregating and non-aggregating cultures, respectively. Interaction times in aggregating and non-aggregating cultures differ by a factor of 1.5 or 2 considering the unbiased estimation, which in comparison is little.

In the macroscopic setup, we observed a distinct difference between the aggregating and non-aggregating culture. In the aggregating culture, aggregates started to form after 20 minutes to 2 hours and only few individual filaments were observed after 2 to 4 hours. Whereas in the non-aggregating culture, we observed no larger aggregates, but maybe bundles of up to 10 filaments.

At this point, it is not evident how the discovered differences in pair interactions between aggregating and non-aggregating cultures affect aggregate behavior. As the initial encounter rates are greater than detachment rates, bundles of several filaments will quickly appear in both cultures. From present information, it cannot be estimated if the bundles further merge to aggregates of hundreds of filaments. In order to answer this question conclusively, an aggregation model based on single *Trichodesmium* filaments and obtained experimental kinetic parameters must be created.

## 4.5 Strengths and limitations of this study

The parallel setup of macroscopic aggregation control and microscopic imaging of *Trichodesmium* filaments of the same culture allowed us to compare filament pair interactions with macroscopic behavior. We assume, but cannot guarantee, that filaments in the microfluidics chamber and filaments in the macroscopic control setup were in a similar physiological state. Filaments were potentially stressed during the filling process due to high shear rates. Possibly, trichomes perceived a change in nutrient levels, if the pre-filled depletion medium (mYBCII medium without Fe and P) was not completely exchanged.

Filament pairs were successfully segmented by the images analysis pipeline described above. It is possible to further automatize and improve the implemented algorithms, especially the merging and splitting algorithm. However, for the purpose of this project, the software worked adequately.

The analysis was based on two assumptions: (1) *Trichodesmium* have no means to measure filament density, i.e. no quorum sensing capabilities, and that therefore separation times are independent of concentration. (2) Filaments behave similarly in filament pairs as in aggregates. It might be worthwhile to further investigate these assumptions. For instance, it has been shown that filaments in aggregates are up to four times as adhesive as single filaments [15]. However, it is not known if a filament actively changes its adhesion once it attaches aggregate or if only more adhesive filaments attach to aggregates in the first place.

The lack of comparable literature makes it difficult to put the obtained results into perspective. A recent study found no significant differences in the mean square displacement (MSD) of single filaments between replete (non-aggregating) and Fe-depleted (aggregating) conditions [15]. The single filament motility pattern (MSD of single filaments in figure C.1) of this study seem to correspond to the findings of [15]. Differences in filament velocity cannot be distinguished clearly

from the MSD. The mean filament gilding speed is with  $2 \mu\text{m s}^{-1}$  substantially higher in [15] than obtained mean filament speeds of  $0.54$  to  $0.67 \mu\text{m s}^{-1}$ .

## 4.6 Aggregate formation in the ocean

Aggregate formation in the ocean is only partially controlled by filament motility. *Trichodesmium* filaments depend on turbulence or vertical migration for encounters. For an average filament concentration of  $2'225 \text{ filaments L}^{-1}$ , as measured in [11], an upper estimate of encounter times in the ocean is between 10 minutes (differential settling) and 3 hours (turbulence) (cf. calculation in appendix F.2). Encounter rates are between 60 hours (turbulence) and 50 days (differential settling) for filament concentrations of  $6 \text{ filaments L}^{-1}$  [11]. Even if two filaments are brought together, they do not necessarily attach to each other. The attachment probability is dependent on encounter angle, shear, respective relative flow velocities and filament adhesion.

However, filament motility influences filament detachment rates and therefore indirectly the minimal filament concentration necessary for aggregate formation. The presented findings could explain the disintegration of existing aggregates, as observed in [15]. Changes in the physiological state of filaments in the aggregate can affect separation probability and filament detachment rate and lead to complete disassembly in the extreme case. Filament detachment rates are further affected by aggregate stability and shear.

## 5 Conclusion

An algorithm to segment *Trichodesmium* filament pairs into the respective single filaments was successfully developed and implemented during this thesis. The segmentation is based on the combination of distance transform and intensity thresholding.

We discovered a novel mechanism of *LOL*-triggered reversals by quantifying *Trichodesmium* filament-filament interactions in aggregating and non-aggregating physiological states. *LOL*-triggered reversals increase filament pair interaction time and are thus a key element in understanding *Trichodesmium* aggregate formation and behavior.

Experimental aggregate formation was not conclusively explained by differences in filament pair interactions in aggregating and non-aggregating cultures. The results indicate that filament pairs in aggregating cultures remain attached longer, but the increase compared to filaments in non-aggregating cultures was limited. As a next step, modeling of *Trichodesmium* filaments using the obtained kinetic parameters as input is necessary to understand aggregates.

The lack of comparable literature made it difficult to verify or falsify the obtained results. It is recommended that some experiments are adapted and repeated to test for experimental artifacts, e.g. residual nutrient levels in microfluidics chambers, hydraulic shear during filling or biased sampling of separation rates.

This thesis focuses on the link between filament-filament interactions and experimental aggregate formation based on quantitative image analysis. It is part of a broader research project by Dr. Ulrike Pfreundt which investigates *Trichodesmium* aggregation with focus on the ocean.

# References

- [1] Letelier, R. M. & Karl, D. M. Role of *Trichodesmium* spp. in the productivity of the subtropical north pacific ocean. *Marine Ecology Progress Series* **133**, 263–273 (1996).
- [2] Bergman, B., Sandh, G., Lin, S., Larsson, J. & Carpenter, E. J. *Trichodesmium* - a widespread marine cyanobacterium with unusual nitrogen fixation properties. *FEMS Microbiology Reviews* **37**, 286–302 (2013).
- [3] Capone, D. G., Zehr, J. P., Paerl, H. W., Bergman, B. & Carpenter, E. J. *Trichodesmium*, a globally significant marine cyanobacterium. *Science* **276**, 1221–1229 (1997).
- [4] Mahaffey, C., Michaels, A. F. & Capone, D. G. The conundrum of marine N<sub>2</sub> fixation. *American Journal of Science* **305**, 546–595 (2005).
- [5] Westberry, T. K. & Siegel, D. A. Spatial and temporal distribution of *Trichodesmium* blooms in the world's oceans. *Global Biogeochemical Cycles* **20** (2006).
- [6] Rodier, M. & Le Borgne, R. Population dynamics and environmental conditions affecting *Trichodesmium* spp. (filamentous cyanobacteria) blooms in the south-west lagoon of New Caledonia. *Journal of Experimental Marine Biology and Ecology* **358**, 20–32 (2008).
- [7] Capone, D. G. *et al.* An extensive bloom of the N<sub>2</sub>-fixing cyanobacterium *Trichodesmium erythraeum* in the central Arabian Sea. *Marine Ecology Progress Series* **172**, 281–292 (1998).
- [8] Hu, C. & Feng, L. GOES imager shows diurnal changes of a *Trichodesmium erythraeum* bloom on the West Florida Shelf. *IEEE Geoscience and Remote Sensing Letters* **11**, 1428–1432 (2014).
- [9] Carlowicz, M. Sea sawdust off Gladstone (2017). Retrieved April 03, 2019 from <https://earthobservatory.nasa.gov/images/91080/sea-sawdust-off-gladstone>.
- [10] Bryceson, I. & Fay, P. Nitrogen fixation in *Oscillatoria (Trichodesmium) erythraea* in relation to bundle formation and trichome differentiation. *Marine Biology* **61**, 159–166 (1981).
- [11] Carpenter, E. J., Subramaniam, A. & Capone, D. G. Biomass and primary productivity of the cyanobacterium *Trichodesmium* spp. in the tropical N Atlantic ocean. *Deep-Sea Research Part I* **51**, 173–203 (2004).
- [12] Chen, Y.-B., Zehr, J. P. & Mellon, M. Growth and nitrogen fixation of the diazotrophic filamentous nonheterocystous cyanobacterium *Trichodesmium* sp. IMS 101 in defined media: Evidence for a circadian rhythm. *Journal of Phycology* **32**, 916–923 (1996).
- [13] Bell, P. *et al.* Laboratory culture studies of *Trichodesmium* isolated from the Great Barrier Reef Lagoon, Australia. *Hydrobiologia* **532**, 9–21 (2005).
- [14] Ohki, K. & Fujita, Y. Aerobic nitrogenase activity measured as acetylene reduction in the marine non-heterocystous cyanobacterium *Trichodesmium* spp. grown under artificial conditions. *Marine Biology* **98**, 111–114 (1988).

- [15] Tzubari, Y., Magnezi, L., Be'Er, A. & Berman-Frank, I. Iron and phosphorus deprivation induce sociality in the marine bloom-forming cyanobacterium *Trichodesmium*. *ISME Journal* **12**, 1682–1693 (2018).
- [16] Rubin, M., Berman-Frank, I. & Shaked, Y. Dust- and mineral-iron utilization by the marine dinitrogen-fixer *Trichodesmium*. *Nature Geoscience* **4**, 529–534 (2011).
- [17] Orcutt, K., Gundersen & Ammerman, J. Intense ectoenzyme activities associated with *Trichodesmium* colonies in the Sargasso Sea. *Marine Ecology Progress Series* **478**, 101–113 (2013).
- [18] White, A., Spitz, Y. & Letelier, R. Modeling carbohydrate ballasting by *Trichodesmium* spp. *Marine Ecology Progress Series* **323**, 35–45 (2006).
- [19] Eichner, M. *et al.* N<sub>2</sub> fixation in free-floating filaments of *Trichodesmium* is higher than in transiently suboxic colony microenvironments. *New Phytologist* **222**, 852–863 (2019).
- [20] Eichner, M. *et al.* Chemical microenvironments and single-cell carbon and nitrogen uptake in field-collected colonies of *Trichodesmium* under different pCO<sub>2</sub>. *The ISME Journal* **11**, 1305–1317 (2017).
- [21] Castenholz, R. W. Aggregation in a thermophilic *Oscillatoria*. *Nature* **215** (1967).
- [22] Polyviou, D. *Nutrient utilisation by Trichodesmium, Characterisation of molecular and physiological Processes*. Ph.D. thesis, University of Southampton (2016).
- [23] Xia, Y. & Whitesides, G. Soft lithography. *Annual Review of Materials Science* **28**, 153–184 (1998).
- [24] SU-8 3000, permanent epoxy, negative photoresist (n.d.).
- [25] Bradski, G. The OpenCV Library. *Dr. Dobb's Journal of Software Tools* (2000).
- [26] Sbalzarini, I. & Koumoutsakos, P. Feature point tracking and trajectory analysis for video imaging in cell biology. *Journal of Structural Biology* **151**, 182–195 (2005).
- [27] Jaqaman, K. *et al.* Robust single-particle tracking in live-cell time-lapse sequences. *Nature Methods* **5** (2008).
- [28] Jones, E., Oliphant, T., Peterson, P. *et al.* SciPy: Open source scientific tools for Python (2001–). Retrieved March 19, 2019 from <http://www.scipy.org/>.
- [29] Mann, H. B. & Whitney, D. R. On a test of whether one of two random variables is stochastically larger than the other. *The annals of mathematical statistics* **18**, 50–60 (1947).
- [30] Kiørboe, T. *A mechanistic approach to plankton ecology* (Princeton University Press, 2008).



# A Overview of experiments

**Table A.1:** Overview of conducted experiments. Experiments 01 to 05 were tests that did not follow the standardized experimental procedure and are therefore not listed.

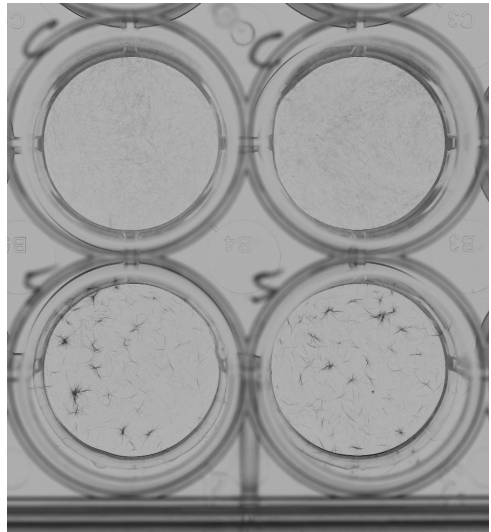
Date	$t_M$ <sup>a</sup>	Start	End	$n_{ch}$ <sup>b</sup>	$n_{pairs}$ <sup>c</sup>	Remarks
06	31.01.2019	08:15	18:11	03:29+1 <sup>d</sup>	4	28 Exp. at night-time. All data was used, as no decrease in mean frame $v_{single}$ was observed. Aggregates in control setup first visible after 20 minutes.
07	01.02.2019	-	10:02	17:02	4	10 Cultures were induced the day before, data was discarded.
08	04.02.2019	08:20	12:18	18:37	4	6 Aggregates in control setup first visible after 2 hours.
10	11.02.2019	08:15	12:44	18:04	4	28 Aggregates in control setup first visible after 45 minutes. Cells died after 2 hours.
11	11.02.2019	19:05	19:30	06:36+1 <sup>d</sup>	4	111 Exp. at night-time. All data was used, as no decrease in mean frame $v_{single}$ was observed. Aggregates in control setup first visible after 45 minutes. Cells died after 2 hours.
12	15.02.2019	08:10	12:13	14:36	4	56 Aggregates in control setup not fully contractile, first visible after 75 minutes.
13	15.02.2019	08:10	15:01	15:27	4	17 Aggregates in control setup not fully contractile, first visible after 2 hours. Experiment too short, data discarded.
14	20.02.2019	08:20	11:03	14:26	8	26 Aggregates in control setup good visible after 1 hour.
15	20.02.2019	08:20	15:12	18:25	8	32 Filaments of aggregating culture in microfluidics chambers started dying after 0.5 h. Aggregates in control setup good visible after 1 hour.
16	27.02.2019	08:25	10:43	14:37	8	98 Aggregates in control setup good visible after 4 hours.
17	27.02.2019	08:25	15:19	19:14	8	17 Filaments of non-aggregating culture in microfluidics chambers started dying after 1 h. Aggregates in control setup good visible after 4 hours.
18	07.03.2019	07:50	11:15	14:59	8	51 Aggregates in control setup good visible after 2 hours.
19	07.03.2019	07:50	15:35	18:54	8	- Filaments did not move, data was discarded.
20	12.03.2019	08:20	12:24	16:14	8	37 Aggregates in control setup first visible after 20 minutes.
21	12.03.2019	12:30	16:51	21:17	8	71 Aggregates in control setup good visible after 1 hour.

<sup>a</sup> Time of Menadione addition

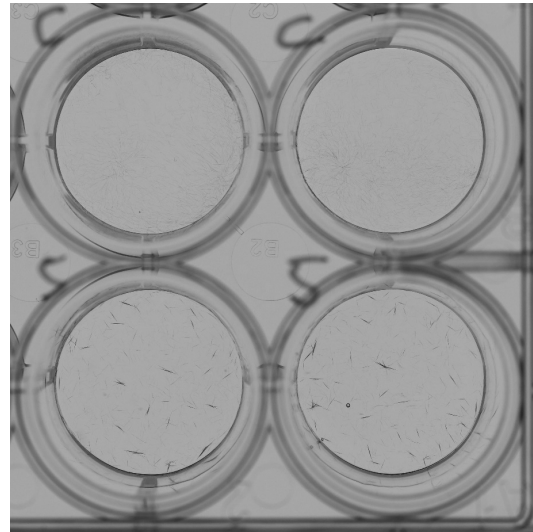
<sup>b</sup> Number of chambers in microfluidics device

<sup>c</sup> Number of observed filament pairs

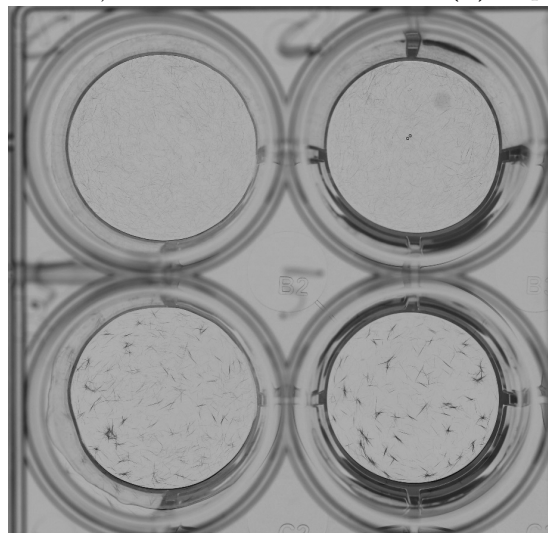
<sup>d</sup> Experiment ended the next day



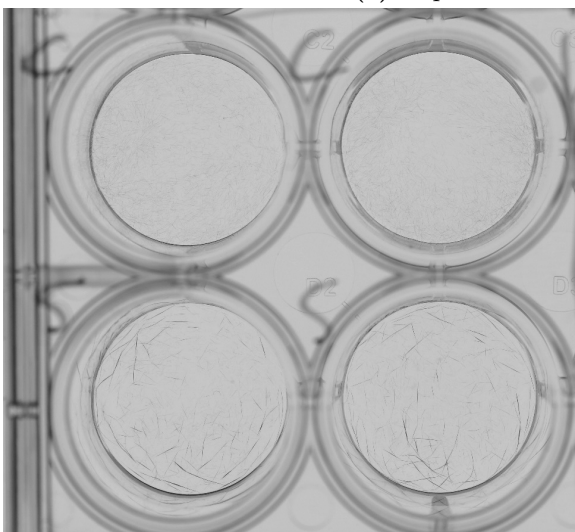
(a) Exp 06 (31.01.2019)



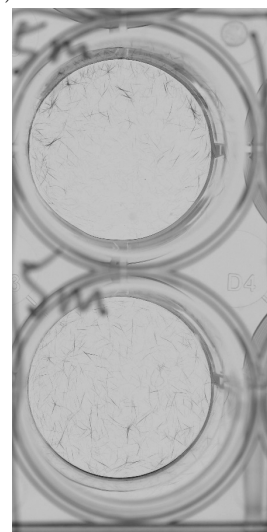
(b) Exp 08 (04.04.2019)



(c) Exp 10 and 11 (11.02.2019)

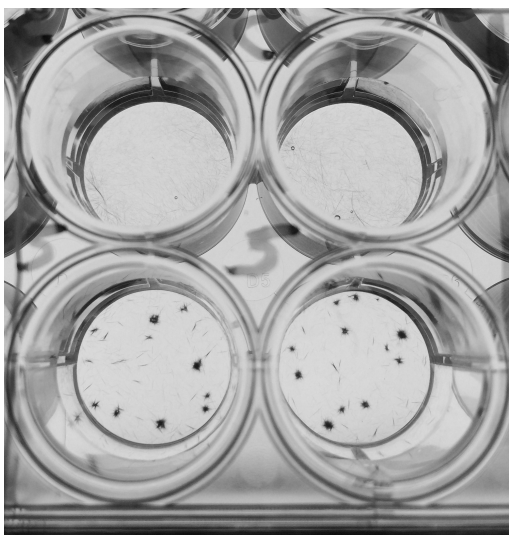


(d) Exp 12 (15.02.2019)

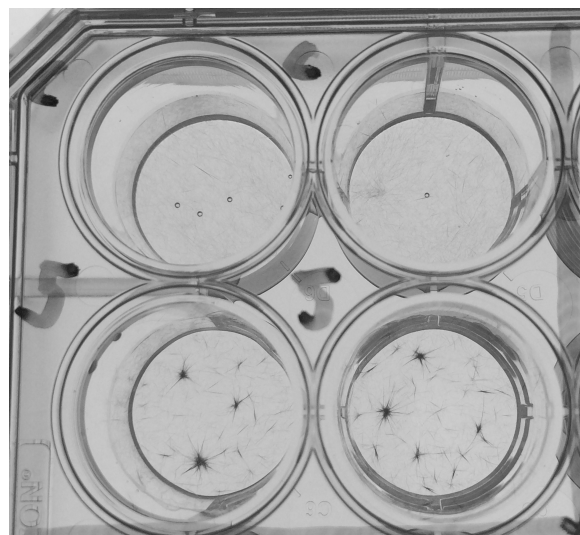


(e) Exp 13 (15.02.2019), Menadione treated samples (top and bottom)

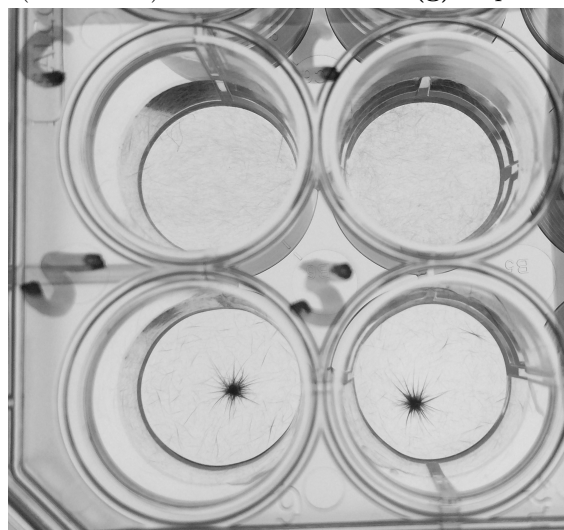
**Figure A.1:** Aggregation control experiments: control (top) and Menadione treated (below) samples.



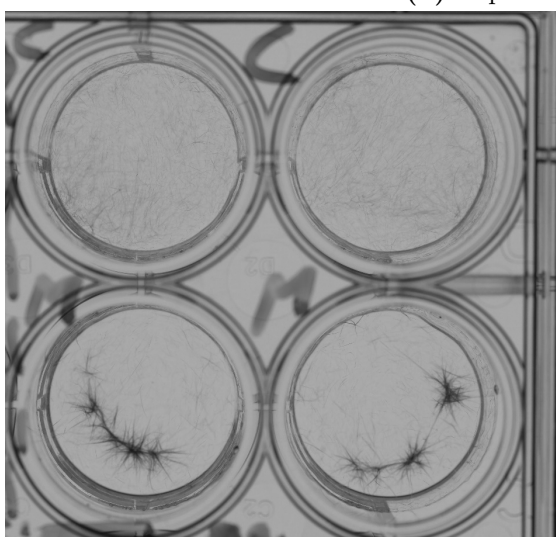
(f) Exp 14 and 15 (20.02.2019)



(g) Exp 16 and 17 (27.02.2019)



(h) Exp 18 and 19 (07.03.2019)



(i) Exp 20 (12.03.2019)



(j) Exp 21 (12.03.2019)

**Figure A.1:** Aggregation control experiments: control (top) and Menadione treated (below) samples (cont.).

## B Distributions of characteristic lengths at reversals points

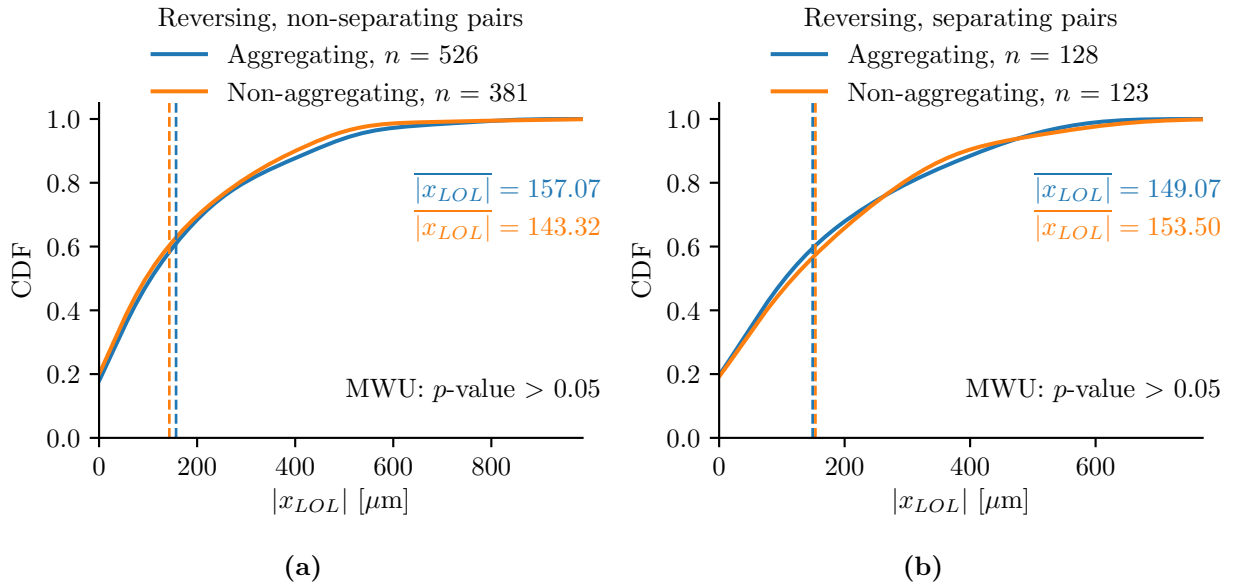


**Figure B.1:** CDF of absolute non-overlap length of shorter filament  $x_{LOL}$  at reversal points of (a) non-separating and (b) separating filament pairs comparing aggregating and non-aggregating cultures. Mean values are indicated with dashed horizontal lines. Fitted distributions and  $p$ -values of the Mann-Whitney- $U$ -test (MWU) are shown on the left.

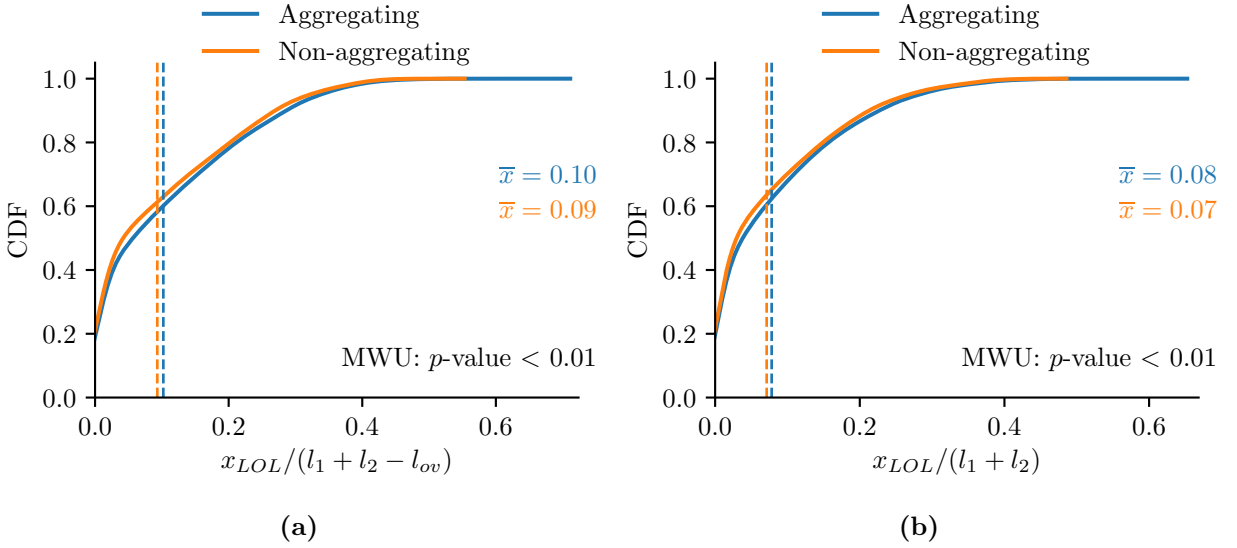


**Figure B.2:** CDF of non-overlap length of shorter filament normalized by (a) total filament pair and (b) summed filament lengths comparing aggregating and non-aggregating cultures. Mean values are indicated with dashed horizontal lines. Fitted distributions and  $p$ -values of the Mann-Whitney- $U$ -test (MWU) are shown on the left.

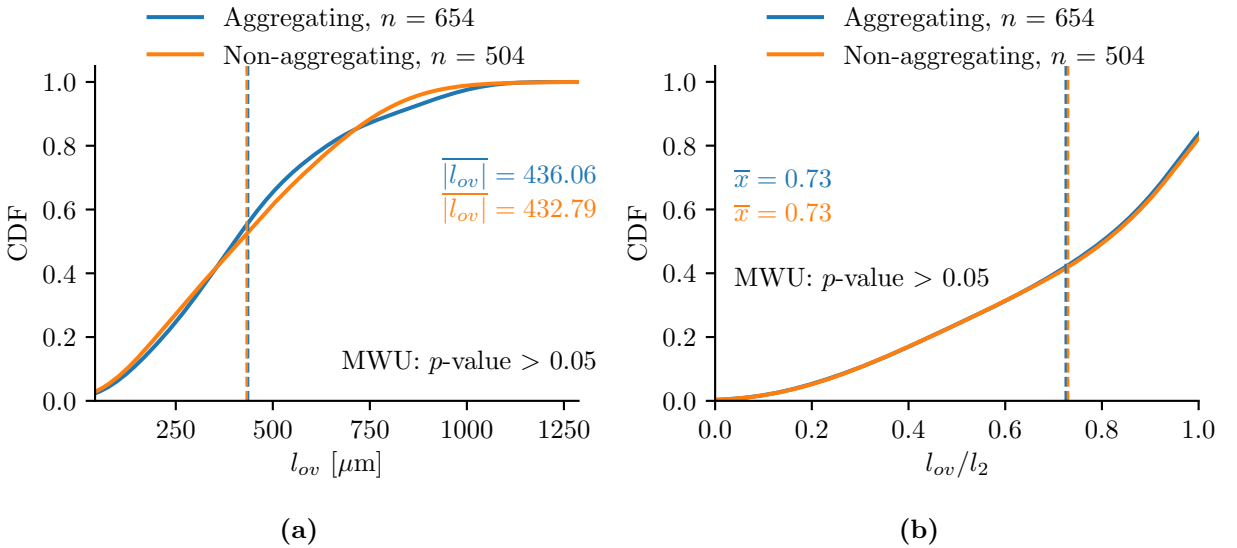


**Figure B.3:** CDF of (a) absolute and (b) normalized overlap length comparing aggregating and non-aggregating cultures. Mean values are indicated with dashed horizontal lines. Fitted distributions and  $p$ -values of the Mann-Whitney- $U$ -test (MWU) are shown on the left.

## C Mean squared displacement of single filaments

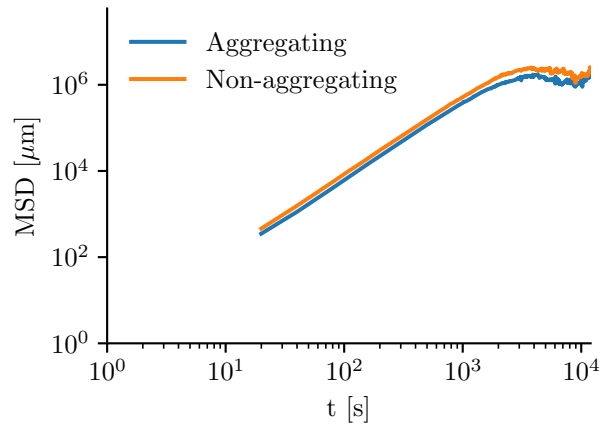


**Figure C.1:** Mean square displacement (MSD) of single filaments. The MSD was averaged for  $t$  bins of 24 s width. Bins with less than four observation are not shown.

## D Distributions of relative filament velocity and interaction time of different subgroups

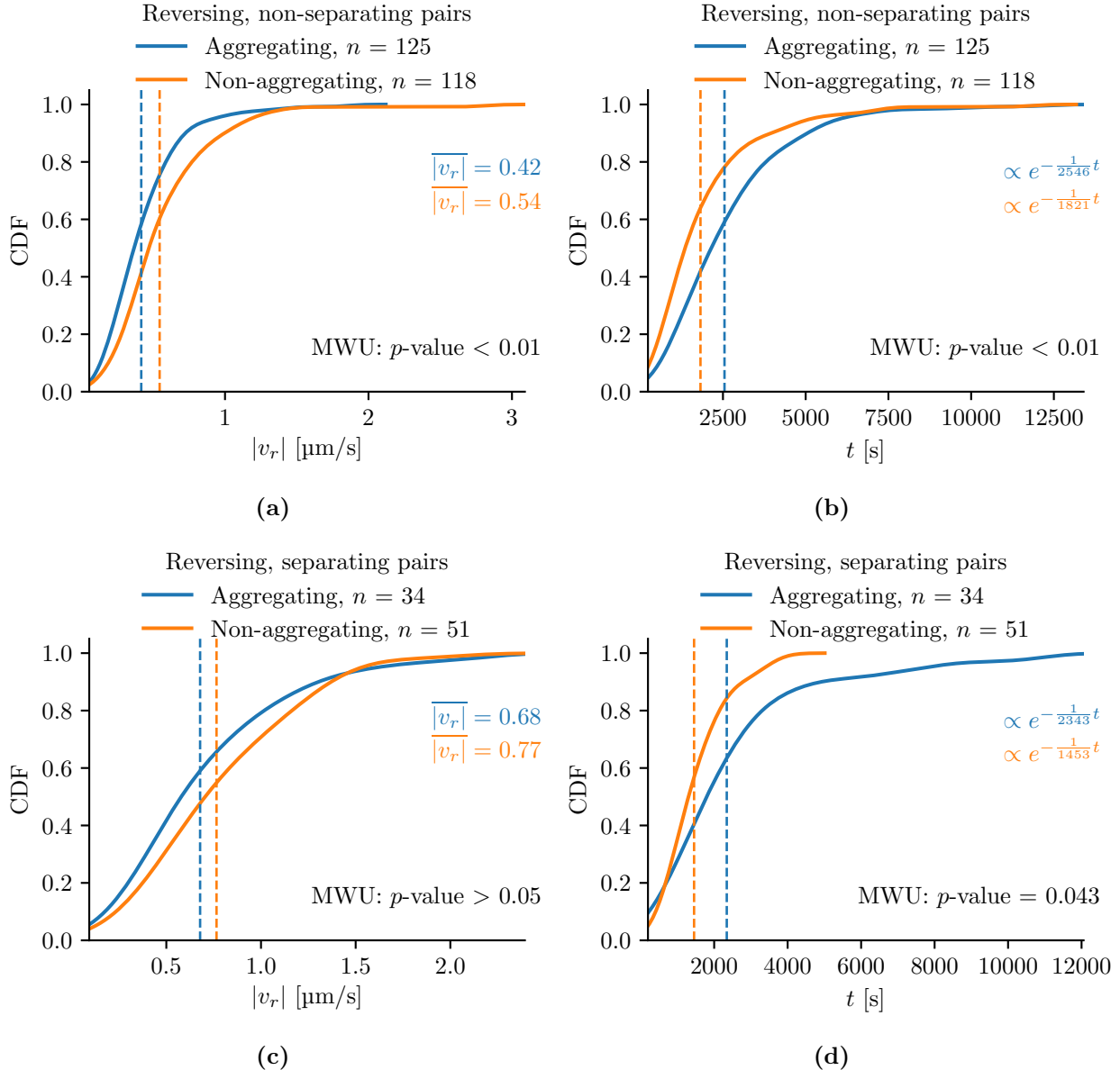


**Figure D.1:** CDF of (a)(c) absolute change in overlap and (b)(d) interaction times of reversing tracks comparing aggregating and non-aggregating cultures. Mean values are indicated with dashed horizontal lines. Fitted distributions and  $p$ -values of the Mann-Whitney- $U$ -test (MWU) are shown on the left.

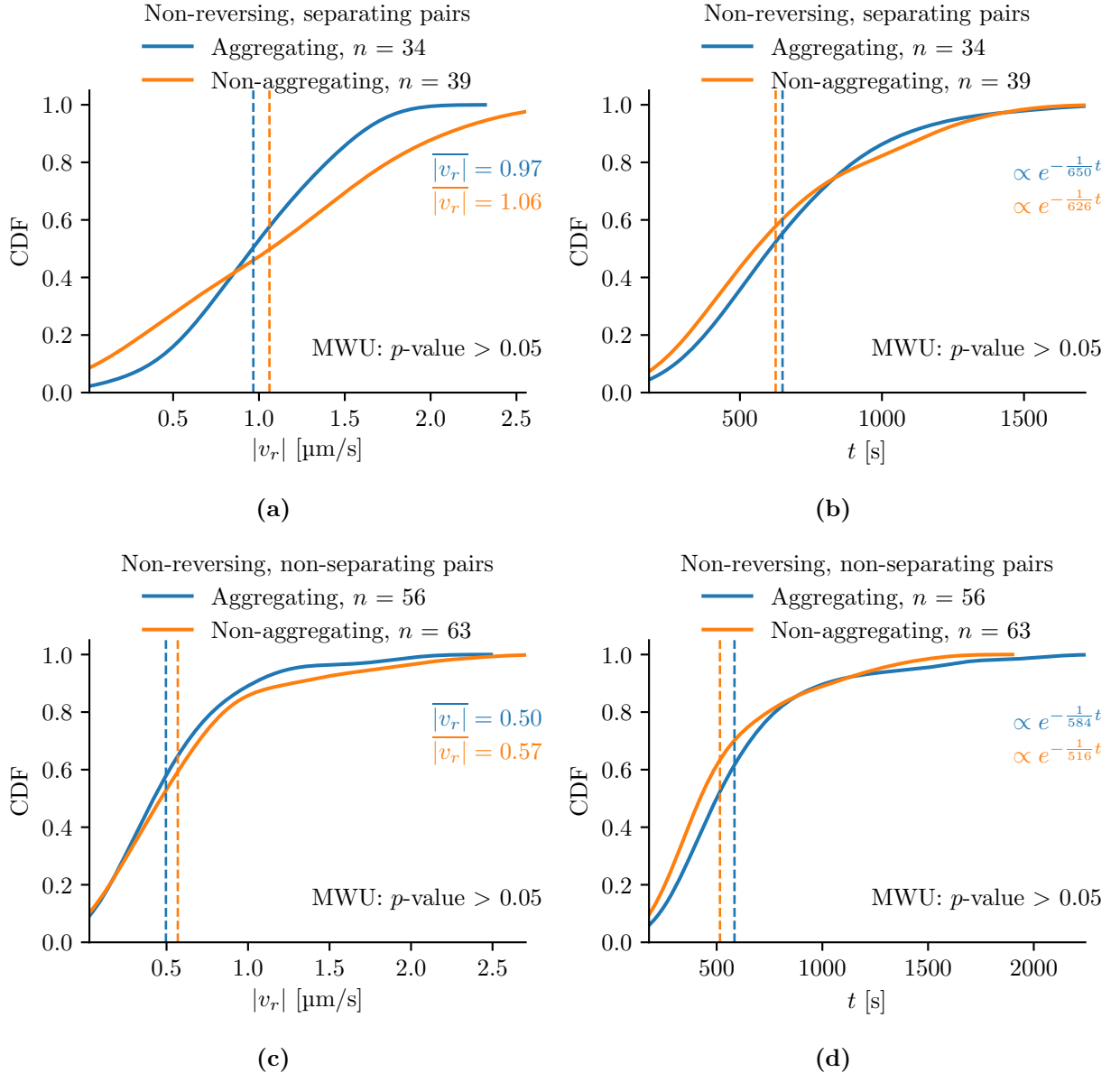


**Figure D.2:** CDF of (a)(c) absolute change in overlap and (b)(d) interaction times of non-reversing tracks comparing aggregating and non-aggregating cultures. Mean values are indicated with dashed horizontal lines. Fitted distributions and  $p$ -values of the Mann-Whitney  $U$  test (MWU) are shown on the left.

## E Interaction time statistics

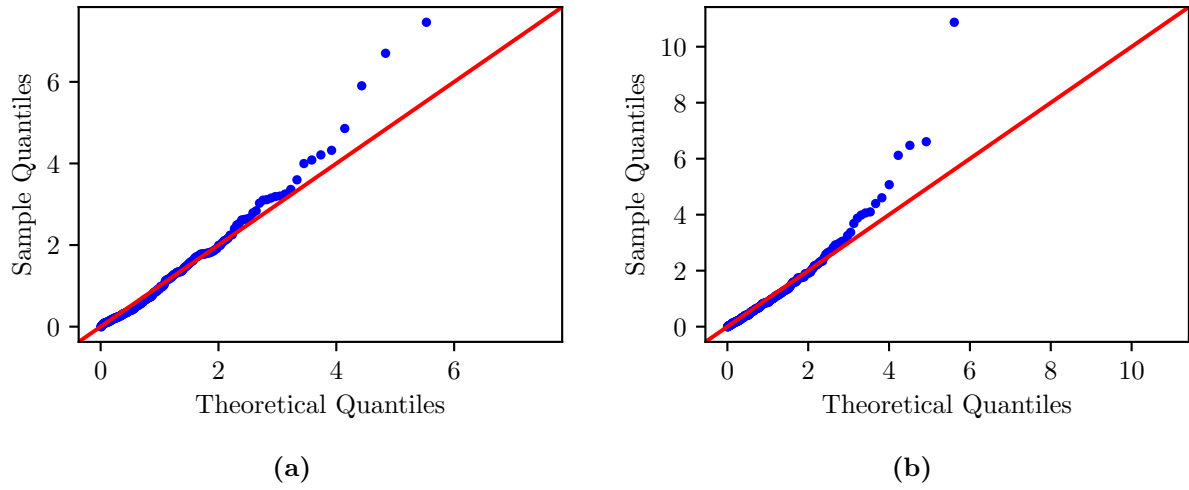


**Figure E.1:** QQ-Plot comparing filament pair interaction times to a exponential distribution for (a) aggregating and (b) non-aggregating cultures.

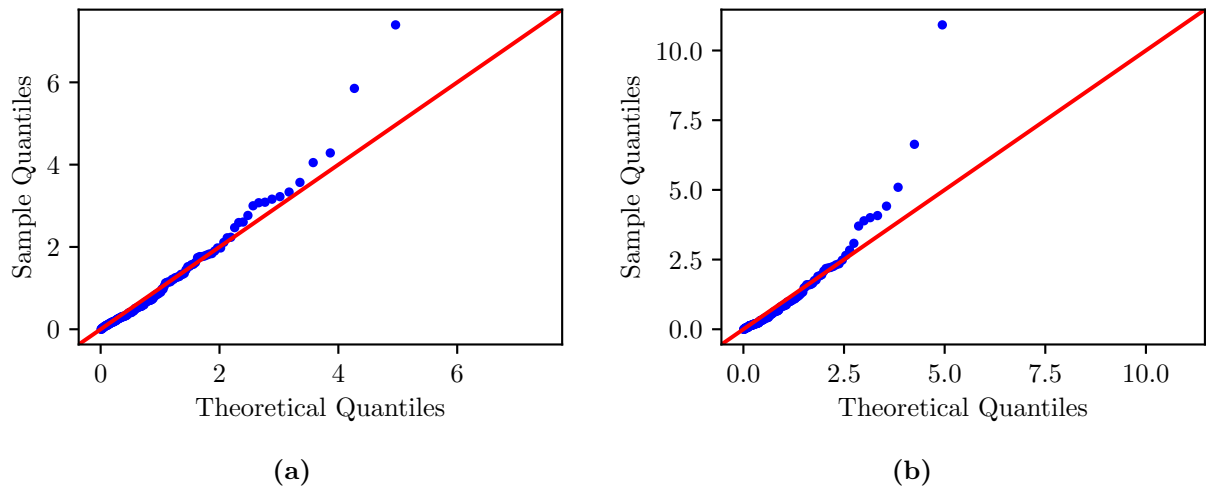


**Figure E.2:** QQ-Plot comparing filament pair merging times to a exponential distribution for (a) aggregating and (b) non-aggregating cultures.

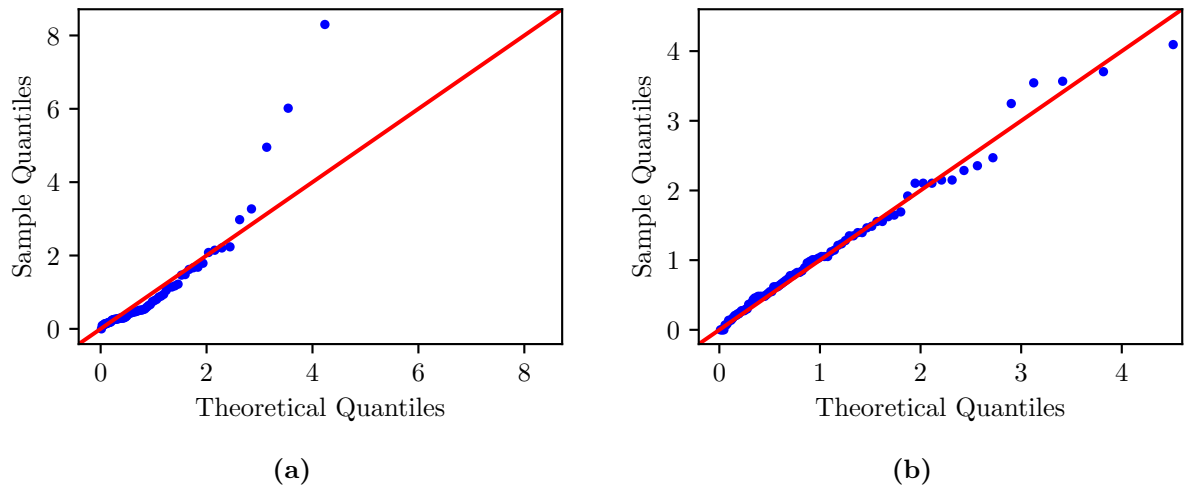


**Figure E.3:** QQ-Plot comparing filament pair separation times to a exponential distribution for (a) aggregating and (b) non-aggregating cultures.

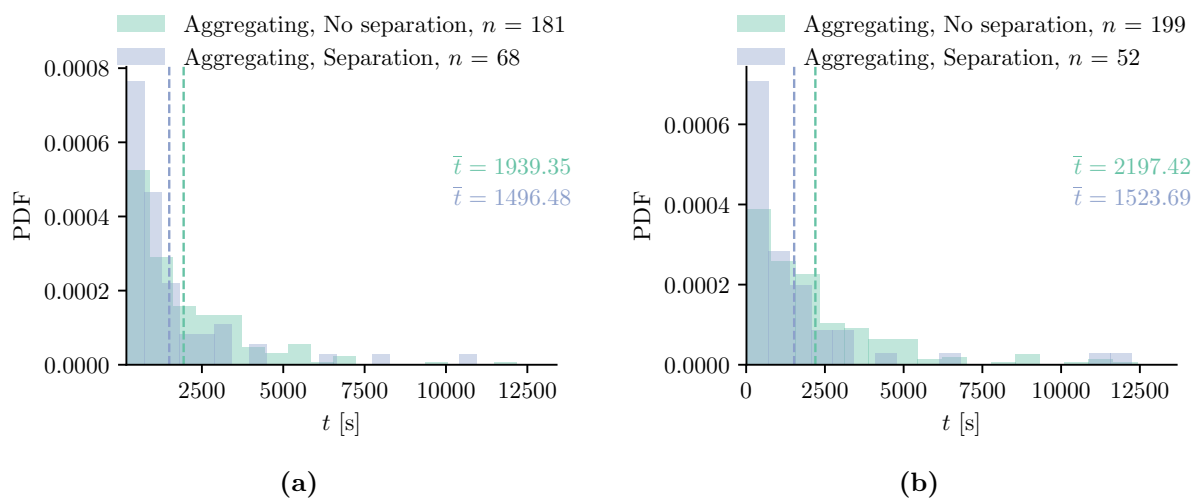


**Figure E.4:** PDF of (a) observed and (b) simulated interaction times of non-separating and separating tracks. Mean values are indicated with dashed horizontal lines and shown on the left.

# F Estimation of *Trichodesmium* encounter rates

## F.1 Aggregation control

The encounter time between any two *Trichodesmium* filaments in the 2D macroscopic set up is controlled by filament motility

$$\tau_{control} = \frac{2A}{lvN_S} = \frac{2 \cdot 2 \cdot 10^8 \mu\text{m}^2}{700 \mu\text{m} \cdot (0.54 - 0.66) \mu\text{m s}^{-1} \cdot 5400 \text{ filaments}} = (195 - 160) \text{ s filaments}^{-1} \quad (\text{F.1})$$

$A$	Well area
$l$	Filament length
$v$	Single filament velocity
$N_s$	Initial number of single filaments

## F.2 In the ocean

Assuming that filaments behave like spheres of radius  $l$ , the encounter time of individual *Trichodesmium* filaments due to turbulent shear in the ocean is [30]

$$\tau_t = (E/n)^{-1} = \left[ \frac{1.3}{2} l^3 n \sqrt{\varepsilon/\nu} \right]^{-1} \quad (\text{F.2})$$

$E$	Encounter rate between filaments
$n$	<i>Trichodesmium</i> concentration
$l$	Filament length
$\varepsilon$	Turbulence intensity
$\nu$	Viscosity

Given observed *Trichodesmium* concentrations between 6000 to 2 225 000 filaments  $\text{m}^{-3}$  [11], average encounter times equal

$$\begin{aligned} \tau_t &= \left[ \frac{1.3}{2} \cdot (0.0007 \text{ m})^3 \cdot (6000 - 2225000) \text{ filaments m}^{-3} \left( \frac{3 \cdot 10^{-8} \text{ W kg}^{-1}}{10^{-6} \text{ m}^2 \text{ s}^{-1}} \right)^{0.5} \right]^{-1} \\ &= 3 \text{ h} - 60 \text{ h} \end{aligned}$$

Encounter times due to differential settling of *Trichodesmium* filaments are given as

$$\tau_s = (N/n)^{-1} = [\pi l^2 (n/2) v] \quad (\text{F.3})$$

$n$  *Trichodesmium* concentration

$l$  Filament length

$v$  Sinking velocity

assuming that one half is neutrally buoyant and the other sinks with velocity  $v$ . With an average sinking velocity of  $0.001 \text{ m s}^{-1}$ , the encounter rates equal

$$\begin{aligned}\tau_s &= \left[ \frac{\pi}{2} (0.0007 \text{ m})^2 \cdot (6000 - 2225000) \text{ filaments m}^{-3} \cdot 0.001 \text{ mm s}^{-1} \right] \\ &= 10 \text{ min} - 50 \text{ d}\end{aligned}$$

Those values are an upper estimate of encounter times in the ocean. In reality, *Trichodesmium* filaments do not behave like spheres of diameter  $l$ , but have a lower equivalent radius.